Nevis-1525
UCR/DØ/96-14
CDF/PUB/TOP/PUBLIC/3681
DØ Note 2957
20th May 1996

The Top Quark

Stephen J. Wimpenny

Department of Physics, University of California, Riverside, California 92521, USA.

Brian L. Winer

Department of Physics, Columbia University, New York, New York 10027, USA.

KEY WORDS: Tevatron, CDF, DØ, Standard Model, Bottom, Higgs

Abstract

Since the discovery of the bottom quark in 1977, physicists have searched for the top quark, the weak isospin partner of the bottom quark. Indirect evidence and estimates of its mass have been made; however, direct observation eluded scientists until recently. In the spring of 1995, two experiments, CDF and DØ, at Fermi National Accelerator Laboratory reported the observation of top-antitop quark pairs created from proton-antiproton collisions. In this report we summarize the experimental status prior to 1995 and discuss the experiments and techniques that in March 1995 resulted in discovery of the top quark. Studies of the top quark's properties, such as its mass and production cross section, are just beginning. We present an overview of the current status of these measurements and perspective on the prospects for the future.

(To appear in Annual Reviews of Nuclear and Particle Science.)

Contents

1 INTRODUCTION

The Standard Model of particle physics unifies the strong and electroweak interactions into a single gauge field theory based on the group $SU(3)_C \otimes SU(2)_L \otimes U(1)_Y$ [1, 2]. An essential element of the model is its family or generation structure in which the fundamental particles are grouped into three parallel families of leptons and quarks (Table 1). Each family consists of two isospin doublets : one lepton doublet and one quark doublet. The discovery of the τ-lepton [3] at the Stanford Linear Accelerator Center (SLAC) in 1977 established the existence of the third lepton generation. The same year, the discovery at Fermi National Accelerator Laboratory (Fermilab) [4] of the *bottom* (b) quark also established the existence of the third quark generation. Once the charge of the b-quark was determined to be $Q_b = -\frac{1}{3}$, it was natural to expect that the missing partner of the doublet should be a quark with charge $+\frac{2}{3}$. Today that partner is known as the *top* or t-quark.

In this paper we review the search for the top quark and its discovery by the CDF (Collider Detector at Fermilab) and DØ collaborations at Fermilab in March 1995 [5, 6]. We begin with an overview of the experimental evidence that supports its existence and summarize the direct and indirect estimates of its mass. The remainder of the article is devoted to a discussion of the CDF and DØ experiments and the discovery of the top quark. We conclude with a review of the current knowledge of the top quark and give a brief perspective on the prospects for future measurements.

1.1 *Indirect Evidence for the Existence of the Top Quark*

The most compelling argument for the existence of the top quark comes from measurements of the weak isospin of the b-quark, I_3^b, which takes values of 0 or $-\frac{1}{2}$ depending on whether the b-quark is in an isospin singlet or doublet state. Within the Standard Model, the bottom quark is expected to be in a doublet state with the top quark being its isospin partner.

Measurements of b-quark decays and the coupling between the Z^0 boson and b-quarks have distinguished between these two alternatives. The results come from low energy processes involving off-mass-shell $Z^0 \rightarrow b\bar{b}$ decays and the study of decays of the Z^0 resonance. The experimental evidence are the forward-backward asymmetry in $e^+e^- \rightarrow b\bar{b}$ [7]; the

absence of flavor changing neutral currents in b-quark decays [8, 9]; the absence of large tree level $B_d^0\bar{B}_d^0$ mixing [10, 11] and the Z^0 partial decay width into $b\bar{b}$ pairs, Γ_b. Of these, the latter is the most powerful measurement, both in precision and because the interpretation of the results is not subject to ambiguities from other gauge bosons (Z') which are predicted in some extensions of the Standard Model. Based on measurements of the ratio of the partial to full hadronic decay width, $R_b = \Gamma_b/\Gamma_{had}$ [12], the partial width for the $Z^0 \to b\bar{b}$ decay is

$$\Gamma_b(Z^0 \to b\bar{b}) = 384 \pm 4 \text{ MeV}, \tag{1}$$

consistent with the value of 381 MeV expected for $I_3^b = -\frac{1}{2}$ and incompatible with the value of 24 MeV expected if $I_3^b = 0$. This provides very strong evidence that the b-quark exists in a weak isospin doublet and therefore provides evidence for the existence of the top quark.

1.2 *Indirect Constraints on the Mass of the Top Quark*

There are several indirect constraints on the mass of the top quark, M_t. Measurements of $B_d^0\bar{B}_d^0$ mixing and the decay width of the W boson provide lower bounds, and radiative corrections to the W and Z boson masses provide an upper bound. Additional information comes from the analysis of precision electroweak measurements at the Z^0 resonance and from νN scattering experiments. By assuming the structure of the Standard Model and fitting the mass dependence of measured parameters one can dervie an estimate of value of M_t. Here we summarize the main features of these calculations.

1.2.1 $B_d^0\bar{B}_d^0$ Mixing

Measurements of $B_d^0\bar{B}_d^0$ mixing at the $\Upsilon(4S)$ resonance give a value for the mixing parameter $\chi_d = \Gamma(B_d^0 \to \bar{B}_d^0 + X) \,/\, \Gamma(B_d^0 \to X)$ of 0.168 ± 0.024 [11, 13]. From theory $\chi_d = x_d^2 \,/\, (1 + x_d^2)$ and this is related to the top quark mass via the relation:

$$x_d \approx 0.15 \left[\frac{\tau_B |V_{td}|^2}{3.3 \times 10^{-16}\text{s}}\right] \left[\frac{B_B f_B^2}{(0.14 \text{ GeV})^2}\right] \left(\frac{M_t}{40 \text{ GeV/c}^2}\right)^2 \tag{2}$$

[14]. Translating the measured value of χ_d into a lower bound on x_d corresponds to a lower bound on M_t of 60 GeV/c^2 at the 95% confidence level (CL).

1.2.2 The Decay Width of the W Boson

Although the W decay width, Γ_W, can be determined by direct methods [15], the most precise determination uses a method based on the ratio, R_{exp}, of the cross section × branching ratio for W and Z boson production in $p\bar{p}$ interactions [16]. This is chosen because the ratio of the two cross sections is relatively insensitive to both experimental and theoretical uncertainties. R_{exp} is related to Γ_W through the relation

$$R_{exp} = \frac{\sigma_W \cdot B(W \rightarrow \ell\nu)}{\sigma_Z \cdot B(Z \rightarrow \ell^+\ell^-)} = \frac{\sigma_W}{\sigma_Z} \frac{\Gamma(W \rightarrow \ell\nu)\Gamma_Z}{\Gamma(Z \rightarrow \ell^+\ell^-)\Gamma_W}. \quad (3)$$

The combined result for Γ_W obtained by this method is 2.062 ± 0.059 GeV [17] in excellent agreement with the Standard Model expectation of 2.077 ± 0.014 GeV [18] where the top quark is assumed to be heavier than the W boson so that the decay $W \rightarrow t\bar{b}$ is kinematically excluded. Translating the experimental measurement into an upper bound on Γ_W yields a lower bound of $M_t > 64$ GeV/c^2 at the 95% CL.

1.2.3 Radiative Corrections to the W and Z Boson Masses

Additional information comes from the measurements of the W and Z boson masses, M_W and M_Z, which are sensitive to the top quark mass through one loop radiative corrections. In the Sirlin scheme for the weak mixing angle, $\sin^2\theta_W$ [19] can be expresseded in terms of a correction term Δr to the predicted values of M_W and M_Z:

$$M_W^2 = \frac{A^2}{(1-\Delta r)\sin^2\theta_W} \quad (4)$$

and

$$M_Z^2 = \frac{4A^2}{(1-\Delta r)\sin^2 2\theta_W}, \quad (5)$$

where $A = (\pi\alpha\sqrt{2}G_F)^{1/2}$ and Δr represents the effect of one-loop radiative corrections [20, 21]. While the dependence of Δr on the mass of the Higgs boson, M_H, is weak [22], the dependence on the top quark mass becomes important once M_t becomes large. Calculations using the measured W and Z masses prior to the startup of the e^+e^- colliders at the Z^0 resonance (LEP and SLC) result in an upper bound of $M_t \leq 200$ GeV/c^2 at the 95% CL [23].

1.2.4 Combined Fits to Electroweak Data

Since 1990 there have been major improvements in the precision of the electroweak parameters. By using data from LEP, SLC and νN scattering, it has been possible to extend the previous analyses and exploit the mass dependence of other electroweak parameters. Several such analyses have been performed, leading to estimates of the value of M_t in the range $150 \leq M_t \leq 210$ GeV/c^2, where the variation comes predominantly from the uncertainty in the value of the Higgs boson mass [12, 24, 25]. Taking a nominal Higgs mass of 300 GeV/c^2, the corresponding result for the top quark mass is

$$M_t = 178\ ^{+11}_{-11}\ (\text{stat})\ ^{+18}_{-19}\ (\text{syst})\ \text{GeV/c}^2, \tag{6}$$

where the first error is the statistical error from the fit, and the second is the additional uncertainty from varying M_H. A feature of some of these analyses [24] is that, if M_H is left as a free parameter, the fits show a preference for small values of M_H close to the present experimental lower bound of 58 GeV/c^2 [26]. This also leads to results for M_t which are around 20 GeV/c^2 lower with somewhat smaller errors. For example, recent fits by Ellis, Fogli and Lisi [27] and Chankowski and Pokorski [28] which impose no M_H constraints, give results of $M_t = 156\ ^{+14}_{-15}$ GeV/c^2 and 156 ± 11 GeV/c^2, respectively.

1.3 *Top Quark Searches at e^+e^- Colliders*

The cleanest signal for top quark production below the W^+W^- threshold would be $t\bar{t}$ pair production in e^+e^- collisions. However, because the beam energies at current machines are too low to produce $t\bar{t}$ pairs, searches have only provided limits on M_t which are restricted in

reach to approximately $\sqrt{s}/2$. Two different techniques have been used to search for top quark production. The first uses the cross section ratio

$$R = \frac{\sigma(e^+e^- \rightarrow \text{hadrons})}{\sigma(e^+e^- \rightarrow \mu^+\mu^-)} = \frac{\sigma(e^+e^- \rightarrow \sum q\bar{q})}{\sigma(e^+e^- \rightarrow \mu^+\mu^-)} = 3\sum Q_q^2, \qquad (7)$$

which should show a jump of $\Delta R = 3Q_t^2 = \frac{4}{3}$ units at the $t\bar{t}$ threshold. The second uses the event shape. The lighter quark pairs are produced back-to-back carrying the total center-of-mass energy and thus give rise to highly collinear events. In contrast, near the $t\bar{t}$ threshold, a heavy top quark pair is produced practically at rest. Each top quark will then decay into three partons ($t \rightarrow Wb, W \rightarrow \ell\nu$ and $u\bar{d}, c\bar{s}$), giving rise to more spherical (isotropic) events.

Although both methods have been used, the second technique has proven the most sensitive and gives the best limits. From the machines operating below the Z boson mass, the tightest limits come from the experiments at TRISTAN [29] which give a lower bound of $M_t > 30$ GeV/c^2 at the 95% CL. More recently experiments at SLAC and CERN [30, 31] have raised this to $M_t > 46$ GeV/c^2 at the 95% CL which is the strongest limit available from current e^+e^- searches.

2 TOP QUARK PRODUCTION AT $p\bar{p}$ COLLIDERS

The mass region above 46 GeV/c^2 has been searched by the experiments at the CERN and Fermilab $p\bar{p}$ Colliders. Because of their higher center-of-mass energy, these are the only machines capable of extending studies into this region. Unlike the e^+e^- analyses, which are comparatively straight forward because of low background, the $p\bar{p}$ searches are complex and require careful attention to the many competing background processes.

In a $p\bar{p}$ collider top quarks can be produced either singly or as a $t\bar{t}$ pair. Single quark production proceeds through the weak interaction and, depending on the value of the top quark mass, proceeds predominantly through either s- or t-channel W boson production ($p\bar{p} \rightarrow t\bar{b} + X$ or $p\bar{p} \rightarrow tq + X$). In contrast, $t\bar{t}$ pair production proceeds via the strong interaction through either gluon-gluon ($gg \rightarrow t\bar{t}$) or quark-antiquark fusion ($q\bar{q} \rightarrow t\bar{t}$). The production cross sections for the strong processes have been calculated in next-to-leading order Quantum Chromodynamics (QCD) to a precision of $\sim$ 20% [32] whereas the cross

section for low mass single t-quark production can be predicted somewhat more precisely using the branching fractions and measured rates for $p\bar{p} \rightarrow W + X \rightarrow e(\mu)\nu + X$ [33, 34]. For large values of M_t, the t-channel process dominates single t production. However, at present, the calculations are still incomplete (see Section 2.3).

2.1 *Low Mass Single Top Quark Production*

If the top quark mass were below ~ 86 GeV/c^2 ($M_W + M_b$), then the $W \rightarrow t\bar{b}$ decay would be the dominant mode at the CERN Sp$\bar{p}$S Collider energy of $\sqrt{s} = 0.63$ TeV. During the mid-late 1980's, searches performed by the UA1 and UA2 collaborations focussed on searching for top through this decay mode. Using the semileptonic decay $t \rightarrow b\ell^+\bar{\nu}_\ell$ as a signature and searching for either $e(\mu)\nu + \geq 2$ jets or $\ell^+\ell^-\nu +$ jets ($\ell = e$ or μ) events, no signal was observed, resulting in a mass limit of $M_t > 69$ GeV/c^2 at the 95 % CL [35]. In 1992 a new analysis of data by the CDF collaboration at the Fermilab Tevatron Collider ($\sqrt{s} = 1.8$ TeV), which was sensitive to both the single top and top quark pair production, raised the mass limit to $M_t > 91$ GeV/c^2 at the 95% CL [36]. This kinematically excluded the production of single top quarks in the decay of an on-mass-shell W boson.

2.2 *$t\bar{t}$ Pair Production*

At the Tevatron energy of 1.8 TeV, $t\bar{t}$ pair production is predicted to be the dominant mode for top quark production. Two strong processes ($gg \rightarrow t\bar{t}$, $q\bar{q} \rightarrow t\bar{t}$) contribute with the $q\bar{q}$ subprocess dominating for top quark masses above ~ 100 GeV/c^2 (see Figure 1). The combined $t\bar{t}$ pair cross section as a function of M_t has been calculated exactly to $O(\alpha_s^3)$ using perturbative QCD [32, 37] and with estimates of the $O(\alpha_s^4)$ and higher order corrections by using soft gluon resummation techniques [38-40]. Inclusion of the higher order corrections increases the cross section by $\sim 30\%$ relative to the exact $O(\alpha_s^3)$ calculations. The resulting predictions for the cross section at $\sqrt{s} = 1.8$ TeV are shown in Figure 2.

The Standard Model predicts that a massive top quark decays with $\sim 100\%$ branching fraction into a real W boson and a b-quark so that $t\bar{t}$ production is characterized by events containing the decays of two W's

and two b-quarks:

$$t\bar{t} \rightarrow W^+ b W^- \bar{b}. \tag{8}$$

The experimental searches at the Tevatron are based on three categories, depending on the different W decay modes. These are referred to as the dilepton, lepton + jets and the all-jets channels. With the exception of the all-jets channel, the searches focus on the presence of one or more isolated, high transverse momentum electrons or muons, and a substantial amount of missing transverse energy from the neutrinos, which escape undetected. Because of the difficulty in the identification of τ decays at hadron colliders, the $t\bar{t}$ decays involving τ-leptons and neutrinos were treated as corrections to the other channels. However, studies in which the τ decay modes are explicitly identified are in progress, and preliminary results have recently been presented. The experimental definition of each search channel is given in Table 2 together with a list of the contributing $t\bar{t}$ decays and their Standard Model branching fractions.

2.2.1 Results from the 1992-1993 Tevatron Collider Run

Between the summer of 1992 and the spring of 1993, data were taken by the DØ and CDF experiments at the Tevatron collider. For DØ this was the first run, and for CDF it was the first run with an upgraded detector. In this section, we summarize the results from this run which paved the way for the top quark observation two years later.

The DØ collaboration performed two separate analyses using 14 pb^{-1} of data. They first looked for dilepton and lepton + jets events consistent with $t\bar{t}$ production in the mass range $M_t > 90\ \mathrm{GeV/c^2}$. Three candidate events (1 $e\mu$, 1 ee and 1 e + jets) were observed with a predicted background of 5.9 ± 2.5 events, consistent with no signal. Interpreted in terms of a limit on $t\bar{t}$ production, this corresponds to a mass limit of

$$M_t > 128\ \mathrm{GeV/c^2} \tag{9}$$

at the 95% CL [41, 42]. Figure 3 shows the DØ 95% CL limit on the $t\bar{t}$ cross section, with the resummed next-to-leading order QCD $t\bar{t}$ cross section shown for comparison.

Based on the limit set by the first analysis and the corresponding results from the CDF collaboration (see below), a second analysis was performed which focused on the high mass region $M_t > 120\ \mathrm{GeV/c^2}$.

This included results from additional decay modes which were insensitive to lower mass events. Seven decay modes were studied: three dilepton channels (ee, $\mu\mu$, $e\mu$), two lepton + jets channels (e + jets, μ + jets) in which toplogical analysis was performed (topological tag), and two lepton + jets channels (e + jets, μ + jets) in which an additional muon compatible with either a $b \rightarrow c\mu\nu$ or a $b \rightarrow c + X, c \rightarrow s\mu\nu$ decay was observed ($b \rightarrow \mu$ tag). A total of nine candidate events were observed with a predicted background of 3.8 ± 0.9 events. No clear signal was observed in any channel (see Table 3) [42, 43]. The small excess of events over background is statistically consistent with both no $t\bar{t}$ signal and the predicted $t\bar{t}$ pair cross section from QCD [38]. Figure 4 shows the resulting cross section measurement compared with the QCD predictions for the mass region $140 < M_t < 200$ GeV/c^2. For a top quark mass of 180 GeV/c^2, this corresponds to a pair production cross section of

$$\sigma_{t\bar{t}} = 8.2 \pm 5.1 \text{ pb.} \tag{10}$$

During the same run, the CDF detector recorded 19 pb^{-1} of data and performed $t\bar{t}$ searches in the dilepton and lepton + jets channels where the latter required that at least one of the b-quark decays was explicitly identified, or tagged, by having either a displaced vertex or a detectable $b \rightarrow c\ell^-\bar{\nu}_\ell$ decay (where $\ell = e$ or μ) (see Table 4). Twelve events were observed, with three of the events satisfying both the displaced vertex requirement and the $b \rightarrow c\ell^-\bar{\nu}_\ell$ requirement. Again, no single channel contained a signal of sufficient significance to establish that $t\bar{t}$ production was observed. However, the combined data were compatible with background at a probability of less than 2.6×10^{-3}. In addition, two pieces of evidence pointed toward the excess being caused by $t\bar{t}$ production. First, a jet in a dilepton event was tagged as a b-quark jet by both tagging methods. Second, analysis of the events from lepton + jets search showed evidence for a mass peak in the region of 175 GeV/c^2, when the events were interpreted as $t\bar{t}$ candidates (Figure 5). A full mass analysis of the events yielded a value of

$$M_t = 174 \pm 10 \text{ (stat)} \, ^{+13}_{-12} \text{ (syst) GeV/c}^2 \tag{11}$$

[44]. Altghough consistent with the predicted $t\bar{t}$ rate, the experimentally measured cross section was somewhat higher than predicted by theory [38]. For the fitted value of M_t, the production cross section was

$$\sigma_{t\bar{t}} = 13.9 \, ^{+6.1}_{-4.8} \text{ pb.} \tag{12}$$

Given the large statistical uncertainties of the measurements, the results from the two experiments are consistent.

2.3 *High Mass Single Top Quark Production*

For top quark masses above 150 GeV/c^2, initial calculations of the cross section for single t ($\bar{t}$) production indicate that the rate may be as much as 1-2 pb for large values of M_t ($\geq$ 170 GeV/c^2) [45, 46]. The events arise through either s- or t-channel W boson production, with small additional contributions from fusion processes such as $gb \rightarrow W^- t$ and $qg \rightarrow q' t \bar{b}$. Of these, the t-channel processes give the largest contributions to the cross section.

Although the lowest order calculation of the cross section for these processes is complete, calculations of the higher order corrections are still in progress. These suggest that the total t or $\bar{t}$ cross section for the high mass region could be as high as $\sim$ 1.8 pb [45]. Studies of the kinematics of such events and more complete calculations are in progress and should be available in the near future [46]. Experimental searches for events of this type have just begun, and results are not yet available.

3 ACCELERATORS AND DETECTORS

3.1 *The Tevatron Accelerator*

The Fermilab accelerator complex ([47] and references therein) is shown schematically in Figure 6. Protons are accelerated in a multistage process by using a linear accelerator, a small booster ring, and a ring of conventional magnets in the main Fermilab tunnel. The Tevatron, a ring of superconducting magnets, performs the final stage of the acceleration. Antiprotons are created by the collision of protons into a metal foil target. The antiprotons are collected, stochastically cooled, and stored in the antiproton accumulator ring. When a sufficient number ($\approx 10^{11}$) antiprotons have accumulated, they are injected into the Tevatron.

In the Tevatron, protons and antiprotons are restricted to bunches, six of each type, and the beam energies are raised from 150 to 900 GeV. Close to each of the interaction regions, the beams are focused to give a beam spot size of $\sim$40 μm at the interaction points. During the 1994-1995 run, proton and antiproton bunches cross once every 3.5 μs, and the accelerator delivered instantaneous luminosities of up to $\sim 2 \times 10^{31}$cm^{-2}s^{-1}. For the combined 1992-1993 and 1994-1995 runs (Run I),

the Tevatron delivered more than 150 pb^{-1} of integrated luminosity to both CDF and DØ.

3.2 *Detectors*

The CDF and DØ detectors are large, general purpose facilities that study many aspects of $p\bar{p}$ collisions. Although the two detectors are considerably different in construction and the technologies they employ, the essential features of the particle detection and identification systems are very similar. The detectors rely on particle track finding devices near the interaction point, hermetic calorimeters outside the tracking chambers, and a muon detection system outside the calorimeters. The detectors have evolved over their lifespan and will continue to evolve in the future. In the following sections, we give a brief overview of each detector as it was configured for the 1994-1995 run and focus on the portions that played key roles in the top quark discovery. More complete discussions of the DØ and CDF detectors can be found in References 48-50 and references therein.

3.2.1 The CDF Detector

The CDF detector is the older of the two facilities. It first observed $p\bar{p}$ collisions in 1985 and has collected data during all of the subsequent Tevatron runs. The CDF detector as it existed for the 1992-1993 and the 1994-1995 runs, is shown in Figure 7.

The CDF tracking system is located inside a solenoid that produces a 1.4 T magnetic field parallel to the beam direction. This is surrounded by the calorimeter system, which is divided into electromagnetic and hadronic sections. Finally, a muon detection system is located behind the calorimeters. The detector readout is controlled by a multilevel trigger which reduces the event rate from 300 kHz to $\sim$ 5-10 Hz which is stored for off-line processing.

The tracking system starts with a four layer single sided silicon-microstrip detector (SVX) [50]. The device is a barrel 51 cm long. However, because of the size of the luminous region ($\sigma \sim 30$ cm), the geometrical acceptance of the device is only 60%. The strip pitch is 60 (55) μm on the inner 3 layers (outer layer). The single hit resolution of the device is 13 μm, and the impact parameter resolution is $\sim$15 μm for high P_T tracks. In top decays, secondary vertices from long-lived

baryons and mesons with heavy quarks (b, c) can be located with an average precision of 130 μm. Outside the SVX is a vertex drift chamber (VTX) which is used to locate the interaction point along the z-axis (beam axis). The SVX and VTX are surrounded by the central tracking chamber (CTC), which has an active volume of 320 cm length and an inner (outer) radius of 31 (132) cm. Tracks are reconstructed in the CTC to provide information both the plane transverse to the beam axis $(r-\phi)$ and along the beam direction (z) and consequently, a momentum measurement due to the presence of a magnetic field. The momentum resolution for the CDF tracking system is $\delta P_{\rm T}/P_{\rm T} = [(0.0009P_{\rm T})^2 + 0.0066)^2]^{1/2}$ where $P_{\rm T}$ is in GeV/c.

The calorimeter system covers the preudo-rapidity (η) region $|\eta| < 4.2$ (η = -ln tan($\theta/2$), where θ is the polar angle with respect to the proton beam). The central electromagnetic (CEM) section has lead absorber and scintillator plates, which are connected to wavelength-shifting bars and read out by phototubes. Behind this are the central hadron (CHA) and wall hadron calorimeters (WHA), both consisting of steel absorber and scintillator plates. In the central region, the energy resolution is $\approx 14\%/\sqrt{E}$ for electrons and $\approx 50(75)\%/\sqrt{E}$ for isolated pions. In the forward/backward direction ($1.1 < |\eta| < 4.2$), the calorimeters are gas (Ar-Ethane) proportional chambers with lead absorber for the electromagnetic compartments (PEM,FEM) and steel absorber for the hadronic compartments (PHA,FHA). The electron energy resolution of the forward/backward calorimeters is $\approx 25\%/\sqrt{E}$ and for isolated pions is $\approx 110\%/\sqrt{E}$. The calorimeter segmentation consists of projective towers with $\Delta\eta \times \Delta\phi = 0.1 \times 15^\circ$ in the central region and $\Delta\eta \times \Delta\phi = 0.1 \times 5^\circ$ in the forward region.

The central muon system consists of several subsystems, labeled CMU, CMP, CMX, and FMU in Figure 7. The CMP resides behind an extra 60 cm of steel absorber, and its coverage overlaps with the CMU in 53% of the solid angle within $|\eta| < 0.6$. Collectively, the tracking chambers provide muon coverage out to $|\eta| < 1.0$. In this region, the detectors consist of four layers of drift chambers, which locate a track stub that can be matched with a tracks reconstructed in the central tracking system. The system is used to detect both the high $P_{\rm T}$ muons from W boson decays and the lower $P_{\rm T}$ muons from semileptonic b-quark decays.

3.2.2 THE DØ DETECTOR

The DØ detector is the newer of the two facilities. It was commissioned in 1992 at the start of Run I and went on to record 14 pb^{-1} of data during the 1992-93 run. The detector configuration for the 1992-93 and 1994-95 runs is shown in Figure 8.

The detector has three subsystems: a compact central tracking system for charged track detection and vertex reconstruction; three large uranium liquid argon sampling calorimeters for electromagnetic and hadronic energy measurement; and a muon spectrometer for muon momentum analysis. The data acquisition is controlled by a multilevel trigger system which reduces the event rate from 300 kHz to $\sim$ 2-3 Hz which can be recorded on tape for off-line processing.

The tracking system consists of a vertex drift chamber (VTX), a transition radiation detector (TRD), a central drift chamber (CDC), and two forward drift chambers (FDC). This provides charged particle tracking over the pseudorapidity range $|\eta| < 3.2$ and measures the trajectories of charged particles with a resolution of 2.5 mrad in ϕ and 28 mrad in θ. From these measurements, the position of the interaction point along the beam direction (z axis) can be determined with a resolution of 8 mm. The central tracking system also measures the ionization of the tracks to distinguish single charged particles and e^+e^- pairs from photon conversions.

The calorimeter is a hermetic uranium liquid argon sampling detector contained in three cryostats (one central, CC, and two forward, ECN, ECS) which provide coverage out to pseudorapidity $|\eta| = 4.5$. The calorimetry in each cryostat is divided into three separate sections : one for electromagnetic shower measurement (EM) and two for hadronic shower measurement and containment (FH,CH). The electromagnetic calorimeter is 21 radiation lengths deep and is segmented longitudinally into four sections. The third section (at electromagnetic shower maximum) has a transverse segmentation of $\Delta\eta \times \Delta\phi = 0.05 \times 0.05$, while the other three sections have a transverse segmentation of $\Delta\eta \times \Delta\phi = 0.1 \times 0.1$. The hadronic calorimeter is 7-9 interaction lengths deep and is segmented into four (CC) or five (ECN,ECS) longitudinal layers. Its transverse segmentation is $\Delta\eta \times \Delta\phi = 0.1 \times 0.1$. Energy measurement in the transition region between the CC and EC calorimeters ($0.8 < |\eta| < 1.4$) is supplemented by massless gap detectors which are mounted inside the cryostats (MG), and by scintillation counters (ICD) that are mounted between cryostats. The energy resolution is $\sigma/\sqrt{E} \approx 15\,\%/\sqrt{E}$

for electrons, $\approx 50\ \%/\sqrt{E}$ for single hadrons and $\approx 80\ \%/\sqrt{E}$ for jets (where E is in GeV). For minimum bias events, the energy resolution for either component of the missing transverse energy, $\not\!\!E_{\rm T}$ is 1.1 GeV + $0.02 \times (\Sigma E_T)$, where ΣE_T is the scalar sum of all the transverse energy in the calorimeter.

The muon system consists of three layers of chambers, with magnetized iron toroids located between the first and second layers. The muon spectrometers provide coverage out to pseudorapidity $|\eta| = 3.6$, although for the top search only the central portion ($|\eta| < 1.7$) is utilized since most of the muons from top quark decays lie in the central region. The central, or wide angle muon spectrometer (WAMUS) covers $|\eta| < 1.7$ over the full azimuthal angle except for $|\eta| < 1$ and $225° < \phi < 315°$ where the innermost layer is removed to accommodate the supports for the CC. The innermost WAMUS layer has four planes of proportional wire drift tubes, and the second and third layers have three planes each. The magnetic field in the iron is 1.9 T, orientated transversely to the beam direction, providing momentum measurement with a resolution of $\sigma(1/p) = 0.18(p-2)/p^2+0.008$ where p is in GeV/c. The thickness of the calorimeter plus the iron toroids varies from 14 to 19 interaction lengths and minimizes the background from hadronic punchthrough. In-flight π and K decay background is also negligible because of the compact calorimeters and central tracking volume. The system is used to detect both the high $P_{\rm T}$ muons from W boson decays and the lower $P_{\rm T}$ muons from semileptonic b-quark decays.

4 EXPERIMENTAL SEARCH AT THE TEVATRON

The analyses leading to the discovery of the top quark focused on the search for $t\bar{t}$ pair production through the dilepton and lepton + jets channels (see below). Although the CDF and DØ analyses differ somewhat in detail. their principal features have much in common.

The initial phase of the experimental search consists of simple counting experiments in which the event selection is made and the expected number of events from background sources is estimated. In the absence of $t\bar{t}$ production, the number of observed events should be consistent with the estimated background. However, if $t\bar{t}$ production is present, and the experiment has sufficient sensitivity, the number of events observed in the data will be significantly larger than the estimated back-

ground. By early 1995, both experiments had accumulated sufficient integrated luminosity to be sensitive to a signal corresponding to a production cross section of several picobarns. In this section we discuss the CDF and DØ counting experiments used to observe $t\bar{t}$ production.

4.1 *The Dilepton Decay Channel*

The searches in the dilepton channel are optimized for the decay chain

$$t\bar{t} \rightarrow W^+bW^-\bar{b} \rightarrow \ell^+\nu b\ell^-\bar{\nu}\bar{b}, \tag{13}$$

where ℓ represents either an electron or a muon. This gives the characteristic signature of two isolated, high transverse momentum leptons; missing transverse energy from the two neutrinos; and at least two hadronic jets from the fragmentation and decay of the b-quarks and any initial state gluons. The combined branching fraction for the searches in this channel ($ee + \mu\mu + e\mu$) is $\sim \frac{4}{81}$ because of the experimental requirement that the W bosons decay into e or μ final states. The factor is not exact because of corrections for $W^+ \rightarrow \tau^+\nu_\tau \rightarrow \ell^+\nu\bar{\nu}_\tau\nu_\tau$ decays (see Table 2).

Experimentally this is the cleanest signal, but because of the small cross section × branching ratio, the expected number of events is very small. A consequence is that even very rare background processes must be considered in attempting to establish the signal. The most significant of these come from Z^0 and continuum Drell-Yan production ($Z^0, \gamma^* \rightarrow e^+e^-, \mu^+\mu^-, \tau^+\tau^-$), vector boson pairs ($W^+W^-, W^\pm Z^0$), heavy flavor production ($b\bar{b}$, $c\bar{c}$), and processes in which jets have been misidentified as leptons. The backgrounds involving two real leptons are estimated from the data where possible and from a combination of Monte Carlo simulation and data for processes which have not been measured experimentally ($W^+W^-, W^\pm Z^0$). The fake (or misidentification) background is calculated from the data by convoluting the rate of the actual parent process with a parametrization of the misidentification probability. The accuracy of the resulting calculations is tested on control samples in the data [42, 44] and by varying the selection cuts on the signal event sample [6, 44].

The rejection against these backgrounds is performed primarily by event kinematics. Both DØ and CDF follow the same general strategy, the specifics of which are listed in Tables 5 and 6. In addition, both experiments make invariant mass cuts to exclude dielectron and dimuon

events from the Z^0 pole. CDF requires the azimuthal angle between the $\not\!\!E_T$ and the nearest lepton or jet to be $> 20°$. This reduces backgrounds from $Z^0 \rightarrow \tau^+\tau^-$ and Drell-Yan events in which the $\not\!\!E_T$ is the result of jet mismeasurement. For both the dilepton and lepton + jet searches (Section 4.2) DØ makes a cut on the variable H_T, which is defined as :

$$H_T = \sum_{|\eta| < 2.5}^{\text{Jets}} E_T + E_T^e \tag{14}$$

for the ee and $e\mu$ channels or

$$H_T = \sum_{|\eta| < 2.5}^{\text{Jets}} E_T \tag{15}$$

for the $\mu\mu$ and lepton + jet channels. E_T^e is the transverse energy of the leading electron in the event. This is especially powerful in the rejection of the residual diboson and $Z^0 \rightarrow \tau^+\tau^-$ backgrounds.

From the analysis of the first $\sim$ 67 pb^{-1} of data from Run I, CDF observed a total of six candidate events with an expected background of 1.3 ± 0.3 events (Table 7) [5]. The corresponding analysis by DØ used $\sim$ 50 pb^{-1} and observed three events with a background of 0.65 ± 0.15 events (Table 7) [6]. Figure 9 shows an event display of a striking $e\mu$ event from the DØ analysis [42]. The characteristic topology of two high P_T leptons along with missing energy and jet activity can be clearly seen. Both groups have presented preliminary results based on the full Run I datasets [51, 52]. These are based on $\sim$ 100 pb^{-1} for DØ and $\sim$ 110 pb^{-1} for CDF and are included in Table 7 for comparison with the published results.

4.2 *Lepton + Jets Decay Channel*

The searches in the lepton + jets channel are optimized for the decay chain

$$t\bar{t} \rightarrow W^+bW^-\bar{b} \rightarrow \ell^+\nu bq\bar{q}\bar{b}, \tag{16}$$

where ℓ represents either an electron or a muon and $q\bar{q}$ is a light quark pair, either a $c\bar{s}$ or $u\bar{d}$, from the decay of the second W boson. This gives the characteristic signature of one isolated, high transverse momentum lepton; missing energy from the neutrino; and four jets from the fragmentation of the $q\bar{q}$ pair and the two b-quarks. Because the

branching fraction for the lepton + jets channel ($\sim \frac{24}{81}$) is much larger than that of the dilepton channel ($\sim \frac{4}{81}$), most of the evidence for top quark production comes from these analyses. As with the dilepton channel, the branching fractions are not exact because of corrections $W^+ \rightarrow \tau^+\nu_\tau \rightarrow \ell^+\nu\bar{\nu}_\tau\nu_\tau$ decays (see Table 2).

The challenge of the lepton + jets searches is to separate the $t\bar{t}$ signal from the large background from $p\bar{p} \rightarrow W$ + multijet events and QCD multijet events in which one of the jets has been misidentified as an electron. The cross sections for both processes are much larger than for the expected $t\bar{t}$ signal (e.g. $\sim$ 17 pb for $W+ \geq 4$ jet production). Although a large fraction of the background can be rejected by imposing tight lepton identification and kinematic cuts, a signal to background of $\sim$ 1:5 still remains (see Figure 10) even after requiring at least four high transverse momentum jets ($E_{\rm T}^{\rm Jet} > 15$ GeV). The additional rejection is achieved by a variety of techniques using the $t\bar{t}$ event characteristics and the strengths of the two detectors. Tables 8 and 9 summarize the standard lepton + jet event selection for DØ and CDF, respectively.

4.2.1 b-QUARK TAGGING TECHNIQUES

The first method used to search for the top quark involves identifying the b-quarks from the top quark decay. This has the advantage of identifying the actual decay products of the top quark. One of the W bosons is identified from the primary lepton and the missing transverse energy. In the cases where both b-quarks are identified, the remaining jets are from the hadronic W boson decay and initial or final state gluon radiation.

Two methods are used to identify b-quark jets. The first relies on finding a low transverse momentum electron or muon from the semileptonic decay of a b- or sequential c-quark. The $P_{\rm T}$ of these leptons can amount to several GeV/c. The second method relies on the long lifetime ($\approx$ 1.6 ps) of B hadrons and the large $P_{\rm T}$ of the b-quark. This combination gives rise to a B hadron decay vertex, which can be separated from the primary interaction point of the proton and antiproton. For $M_{\rm t} \sim 175$ GeV/c^2, the average separation is approximately 0.5 cm. This makes it possible to locate displaced vertices on a case-by-case basis by using a precision silicon-vertex detector. Currently, only CDF has such a device, although both detectors will have excellent silicon tracking devices for the next collider run in 1999 (see Section 6).

4.2.2 TAGGING $b \rightarrow \ell\nu X$

Both CDF and DØ have performed searches for additional low P_T leptons in the lepton + jets data. Based on the semileptonic branching fractions, 22% of b-quarks will produce a muon in the final state either directly from its semileptonic decay or from the semileptonic decay of a sequential c-quark. A muon from a c-quark decay, on average, will have lower momentum than one from the semileptonic decay of the b-quark, and the efficiency for finding these muons will be lower. Another 22% of the b-quarks will produce a low P_T electron. The efficiencies for locating a low P_T electron is only about 1/3 of the efficiency for locating a low P_T muon. Candidate leptons must have P_T greater than 2 GeV/c at CDF and 4 GeV/c for the DØ search. No upper limit is placed on the lepton P_T. In principle, some dilepton events could also pass this event selection; however, any events passing the dilepton selection are explicitly removed from the lepton + jets analysis. The DØ analysis imposes the additional requirement of $H_T > 140$ GeV to give optimal rejection against the residual background from W + multijet and QCD multijet events. For both experiments, the total tagging rate of $t\bar{t}$ by one or more low P_T leptons is about 20%.

With this search technique, the backgrounds are similar to those of the dilepton decay channels. For the CDF analysis, the major backgrounds are fake leptons and electrons from unidentified photon conversions. These rates and the smaller $W + b\bar{b}$ and $W + c\bar{c}$ backgrounds are determined directly from inclusive jet data. The remaining backgrounds from diboson production (WW,WZ,ZZ), $Z \rightarrow \ell\ell$ decays, and Drell-Yan production are determined by the same techniques as for the dilepton analyses [44]. For DØ, the higher muon P_T requirement and the H_T cut significantly decrease the fake lepton background, and the $W + b\bar{b}$ and $W + c\bar{c}$ background dominates. This and the other background contributions are calculated by the same methods as in the dilepton analyses [42].

The search results are summarized in Tables 10 and 11 for CDF and DØ, respectively. DØ observes six events with a combined background of 1.2 ± 0.2 [6], and CDF observes 23 b-tags in 22 events with a predicted background of 15.4 ± 2.0 tags [5]. Figure 11 shows the results of the DØ search, plotted as a function of the exclusive jet multiplicity. While the data are consistent with the expected background in the 1 and 2 jet samples, a clear signal excess is visible in the ≥ 3 jet sample. The CDF data shows a similar behavior.

4.2.3 Tagging by a Displaced Vertex

Identifying b-quarks by the presence of a secondary vertex that is displaced from the primary interaction point is a very clean way of locating b-quark jets. This technique will be the primary technique used for future studies of the top quark (see Section 6). It is a cleaner technique than the soft lepton tag discussed above and has the advantage that the false tag rate is small and can be accurately predicted from the data itself. The remaining backgrounds come from non-top events which contain b-quarks. Fortunately their rate is small.

Figure 12 shows a schematic picture of a secondary vertex. A long-lived B hadron will travel a distance L_{xy} measured in the plane transverse to the beam axis[1]. When the hadron decays, the decay particles emanate from the point of decay and will not necessarily point back to the primary vertex. As a result, the decay products have a significant impact parameter (d) (or minimum distance of closest approach) with respect to the primary vertex. The algorithm uses tracks with a significant displacement from the primary vertex ($d/\sigma_d > 3$) to reconstruct the position of the secondary vertex and to measure L_{xy}. The typical uncertainty on L_{xy}, $\sigma_{L_{xy}}$ is $\sim$ 130 μm, but the distribution is broad and extends to 40-50 μm. For an acceptable tag, the secondary vertex is required to be displaced from the primary vertex by more than 3 standard deviations, $|L_{xy}/\sigma_{L_{xy}}| > 3$. Tags with $L_{xy} > 0$ are considered b, c hadron candidates. Tags with $L_{xy} < 0$ come primarily from track mismeasurement and are used to measure the rate of fake tagging due to instrumental effects. The efficiency of the tagging algorithm to identify at least one b-quark jet in a $t\bar{t}$ event is about 40% [5]. The rate of misidentifying a non-b jet within the fiducial volume of the SVX, as a b-quark jet is about 1% or less [44].

The dominant backgrounds to the $t\bar{t}$ search in this channel are $W + b\bar{b}$ and $W + c\bar{c}$ and fake tags, which account for 60% of the total background in this. Other background sources are flavor excitation processes such as $sg \rightarrow Wc$, diboson production (WW, WZ) and $Z \rightarrow \tau\tau$ decays. The rates for these processes are calculated using Monte Carlo simulations except for the fake tag background, which is determined directly from the data [44]. The background predictions are tested in various control samples, one of which is the lepton + jets data itself.

In lepton plus 1 and 2 jet events, the contribution of $t\bar{t}$ events should

[1] The current silicon-vertex detector at CDF only provides information in two dimensions, the directions transverse to the beam (x and y).

be small. Figure 13 shows the number of events before and after b tagging as a function of jet multiplicity. In the control region (the 1 and 2-jet samples), the background prediction agrees well with the observed data. The two jet sample contains some $t\bar{t}$ and single t or $\bar{t}$ events and therefore a slight excess is expected. The signal region, $N_{\rm jet} \geq 3$, shows a clear excess above background. The figure also shows the expected distribution when $t\bar{t}$ production is added to the prediction. In the signal region CDF observe a total of 27 tags with a predicted background of 6.7 ± 2.1 (see Table 10) [5]. The 27 tagged jets occur in 21 events. The six double tagged events are very unlikely to be from any background source. Table 10 also includes the preliminary results for the full Run I analysis.

The power of this technique is illustrated by Figure 14, which shows an expanded view of an e + jets event in the CDF detector. In this event both b-decays have been identified using the displaced vertex technique and appear as well defined secondary vertices. As a cross check of the tagging, the reconstructed invariant mass of the remaining two jets in the event (Jet 2 and Jet 3) is 79 GeV/c^2, consistent with the hypothesis that they come from the hadronic decay of a W boson.

4.2.4 Topological Event Selection

Topological isolation of $t\bar{t}$ events relies on the fact that the jets from heavy top quark decay will be both more centrally produced and more energetic than the jets from W + multijet background. The topological separation performed by DØ and CDF differ from one another, and each is reviewed in turn.

The DØ analysis begins by requiring that there be $\geq$ 4 jets with transverse energy, $E_{\rm T}^{\rm Jet}$>15 GeV, and, to keep this analysis orthogonal to the the $b \rightarrow c\mu\nu$ tag, that there be no additional muon consistent with a semileptonic b- or c-quark decay. Two topological variables $H_{\rm T}$ and Aplanarity ($\mathcal{A}$) are then used to separate the signal and background. $H_{\rm T}$(see Section 4.1) measures the transverse activity in the event and a large value of $H_{\rm T}$ is indicative of the decay of a massive object. The aplanarity measures the activity transverse to the plane of maximum activity and is proportional to the lowest eigenvalue of the momentum tensor for the observed objects. $\mathcal{A}$ takes the value of 0.5 for highly spherical events and 0.0 for planar events. The $t\bar{t}$ events tend to be more spherical than the W + multijet background [42]. Table 8 summarizes the selection cuts used for the analysis. Since a substantial fraction of

the background rejection comes from the H_T requirement, it is essential to demonstrate that the H_T distribution for the background processes is well understood. Figure 15 shows the H_T distributions from the background dominated channels $e + \not\!\!E_T$ + two jets and $e + \not\!\!E_T$ + three jets (E_T^{Jet} >15 GeV). Shown for comparison is the calculated background which includes W + multijet production as derived from a Vecbos Monte Carlo simulation [53], and the misidentification background from QCD multijet production, which is calculated from an independent dataset. The agreement is very good, as is the case for the distributions in $\mathcal{A}$ and the other variables used in the event selection.

In addition to the standard selection cuts (see Table 8), a loose selection was performed in which the H_T cut was removed and the cut on the aplanarity was reduced to 0.03. This selection of events was used to check the accuracy of the background calculations and to provided a less restrictive data sample for mass fitting (Section 5). With these cuts and $\sim$ 50 pb^{-1} the DØ analysis found eight events with an expected background of 1.9 $\pm$ 0.5 events for the standard selection and 23 events with an expected background of 15.7 $\pm$ 3.1 events with the loose selection [6]. The preliminary results from the DØ 100 pb^{-1} analysis are included for comparison [52].

The primary search technique used by CDF relies on the b-quark tagging. However, kinematic analyses have been used to provide a more complete search for $t\bar{t}$ production. CDF has used two different techniques. The first analysis [54] is a likelihood analysis of $W + \geq 3$ jet events in which the transverse energies of the second (E_{T2}) and third (E_{T3}) highest E_T jets are used to differentiate between the $t\bar{t}$ signal and background. The second [55] starts from a sample of $W + \geq 4$ jet events (see Table 9) and uses a transverse energy variable $\mathcal{H}$ to separate the signal and background.

Since the jets from $t\bar{t}$ decays are expected to be emitted at larger angles (θ) than those from directly produced W's with associated jets, each jet is required to have $|\cos(\theta^*)| < 0.7$, where θ^* is the jet polar angle in the center-of-mass frame of the event. Next, an event relative likelihood ($\mathcal{L}$) is formed using E_{T2} and E_{T3} where

$$\mathcal{L} = \frac{\left[\left(\frac{1}{N_{t\bar{t}}}\frac{dN_{t\bar{t}}}{dE_{T2}}\right)\left(\frac{1}{N_{t\bar{t}}}\frac{dN_{t\bar{t}}}{dE_{T3}}\right)\right]}{\left[\left(\frac{1}{N_{bkg}}\frac{dN_{bkg}}{dE_{T2}}\right)\left(\frac{1}{N_{bkg}}\frac{dN_{bkg}}{dE_{T3}}\right)\right]}. \tag{17}$$

This classifies the event as top-like or background-like. Events with $\ln(\mathcal{L}) > 0$ are more consistent with $t\bar{t}$ production than W + multijet

background events. Calculations with the Vecbos [53] Monte Carlo predict that 22 ± 5% of the W + multijet background will have $\ln(\mathcal{L}) > 0$. By assuming that all of the events with $\ln(\mathcal{L}) < 0$ are background and normalizing to the shape of the expected background, a prediction of 7.2 ± 2.1 events is obtained for $\ln(\mathcal{L}) > 0$. From 67 pb^{-1} of data, 25 events had $\ln(\mathcal{L}) < 0$, and a further 22 had $\ln(\mathcal{L}) > 0$ (see Figure 16) [54]. Because the likelihood distribution is derived from Monte Carlo simulations, this technique has uncertainties associated both with the shape of the jet E_{T} spectrum and the detector energy scale. Nonetheless, even with these uncertainties folded into the analysis, the data are consistent with a pure background with a probability of only 0.26% [54].

The second CDF analysis is based on the total transverse energy of the event and uses the variable $\mathcal{H}$ where

$$\mathcal{H} = \sum^{\text{Jets}} E_{\text{T}} + \not\!\!E_{\text{T}} + E_{\text{T}}^{\ell}, \tag{18}$$

which is similar to the variable H_{T} used by DØ, except that the $\not\!\!E_{\text{T}}$ is included. The $\mathcal{H}$ analysis uses the shape of the full $\mathcal{H}$ distribution for the analysis. A Kolmogorov-Smirnov test is performed to test the consistency between the data and the calculated background from W + multijet events. The data are incompatible with a background-only hypothesis (probability $< 1.6 \times 10^{-4}$) [55]. However, when a $t\bar{t}$ component is added, the combined ($t\bar{t}$ + background) distribution agrees reasonably well with the data (see Figure 17) [55]. As with the $\ln(\mathcal{L})$ method, the analysis of the $\mathcal{H}$ distribution has uncertainties associated with the shape of the predicted $\mathcal{H}$ spectra and the detector energy scale. This technique also allows the extraction of the top quark mass and a $t\bar{t}$ production cross section [55]. The values agree with the measurements described in Section 5.

4.3 *Other Decay Channels*

In order to complete the study of top quark decays, it is necessary to investigate other possible decay modes, such as the all-jets mode and explicit τ-decay modes. Preliminary results using the all-jets decay mode have been presented by both collaborations. Two additional decay modes are in the early stages of analysis and preliminary results have been presented. CDF have made an exploratory study of the decay modes explicitly involving τ-leptons and DØ have searched for events

containing electrons and a substantial amount of missing transverse energy.

4.3.1 All-Jets Decay Channel

The signature for the production of $t\bar{t}$ events in the all-jets channel is six (or more) high transverse momentum jets with no significant missing transverse energy, i.e.

$$t\bar{t} \rightarrow W^+bW^-\bar{b} \rightarrow q\bar{q}bq\bar{q}\bar{b}, \tag{19}$$

where the two $q\bar{q}$ pairs are light quark pairs from hadronic decays of the two W bosons (either $c\bar{s}$ or $u\bar{d}$). The large branching fraction for this channel ($\frac{36}{81}$) makes it attractive in terms of the number of $t\bar{t}$ events expected. However, there is a very large background from QCD multijet production that is kinematically quite similar to the $t\bar{t}$ signal. For example, even after requiring that an event contain at least 6 jets ($E_{\rm T}^{\rm Jet} >$ 15 GeV) the signal-to-background ratio is still only $\sim 1/1000$.

Both experiments have presented preliminary results from the analysis of this channel. DØ uses a combination of topological selection and $b \rightarrow \mu$ tagging to reduce the level of the background. For a full description of the variables used and the techniques used to tune the selection cuts, we refer the reader to Reference [52]. After applying strict topological cuts and requiring a single $b \rightarrow \mu$ tag, 15 events survive with an expected background of 11.0 $\pm$ 2.3 events. With a double $b \rightarrow \mu$ tag there are two events with an expected background of 1.4 $\pm$ 0.4 events. DØ determines preliminary $t\bar{t}$ pair cross sections of 4.4 $\pm$ 4.9 pb and 3.9 $\pm$ 9.8 pb for the single- and double-tag analyses, respectively. The results are statistically limited at present but they are in good agreement with the cross sections measured from the other decay channels (Section 5). A determination of $M_{\rm t}$ is in progress, and results are expected to be available soon.

In addition to the 6 jet requirement, CDF requires that the total scalar transverse energy in the event, $\sum E_{\rm T} \geq 200$ GeV, that $\sum E_{\rm T}/\sqrt{s} > 0.75$, and that there be at least one displaced vertex b tag. For a data sample of 110 pb^{-1}, 192 events are observed with an expected background of 140 $\pm$ 14 events. The top mass and cross section are extracted from this analysis. The mass distribution exhibits an enhancement near 180 GeV/c^2 and is consistent with the CDF mass measurement described in Section 5. The $t\bar{t}$ production cross section is found to be

$11.9\ ^{+3.5}_{-4.3}$ pb, at $M_t = 175$ GeV/c^2, consistent with the measurements described in Section 5.

4.3.2 τ-Decay Channels

The CDF collaboration has searched for dilepton modes which explicitly involve the decay of a τ-lepton ($e\tau$ or $\mu\tau$). Two techniques are employed. Both start with events containing a high P_T electron or muon and event selection similar to the standard dilepton analysis (see Section 4.1). The first technique searches for single-pronged hadronic τ-lepton decays by searching for isolated single tracks which are inconsistent with being either an electron or a muon. The second analysis searches for either single- or three-prong τ-decays. This relies on identifying τ leptons by their calorimeter signature. Background events come from both $Z \rightarrow \tau\tau$ decays and events contining jets that fake the τ signature. A preliminary analyses using these techniques finds 4 events with a background of 1.7 ± 0.3 events in the single prong search and 3 events with an expected background of 0.91 ± 0.23 in the combined one and three prong search [51].

4.3.3 The $e + \not{E}_T$ Channel

The DØ collaboration has searched for single electron + $\not{E}_T$ events with a large amount of missing energy ($\not{E}_T > 50$ GeV) and for which the $e + \not{E}_T$ transverse mass is incompatible with most conventional $W \rightarrow e\nu$ decays ($M_T^{e\nu} > 115$ GeV/c^2). This search is sensitive to events from both the $t \rightarrow W^+b \rightarrow e^+\nu b$ and $t \rightarrow W^+b \rightarrow \tau^+\nu b$ decay chains. After applying additional selection cuts to reject events which satisfy the standard DØ dilepton and lepton + jet analyses, two events are observed in 88 pb^{-1} of data. Background events come from both W + multijet and QCD multijet production. A preliminary analysis indicates a background of 1.4 ± 0.4 events and an expected signal from $t\bar{t}$ decays of 1.1 ± 0.1 events for $M_t = 180$ GeV/c^2 [52].

4.4 *Summary of Event Samples*

The results of the published dilepton and lepton + jets counting experiments performed by DØ and CDF are summarized in Table 12.

Both collaborations observe an excess of events in all of the channels studied which is consistent with the expectations for the production and decay of a massive top quark. Table 12 also lists the probability that the number of observed events could be the result of fluctuations in the background. Interpreted in this way, the probabilities for the CDF and DØ observations to come from background fluctuations are 1 $\times$ 10^{-6} and 2 $\times$ 10^{-6}, or 4.8 and 4.6 standard deviations, respectively, for gaussian background distributions.

Taken together, this is overwhelming evidence the two collaborations are observing phenomena that within the context of the Standard Model can only be attributed to the pair production of top quarks.

5 TOP QUARK PROPERTIES

The CDF and DØ counting experiments provide convincing evidence for the production of a massive object which decays through the modes expected for the Standard Model top quark. In order to test the interpretation that the top quark is responsible for the observed signals, both collaborations have measured the production cross section and identified subsets of events for which it is possible to measure the top quark mass. In this section we summarize the results and compare to them the predictions of theory.

5.1 *$t\bar{t}$ Production Cross Section*

A measurement of $\sigma(p\bar{p} \rightarrow t\bar{t})$ provides a test of QCD at the high mass scale associated with the top quark ($Q^2 \approx M_t^2$). The acceptance of the CDF and DØ top searches depends on the value of M_t because of the change in the shape of the lepton and jet Et spectra with increasing M_t. Hence, the $t\bar{t}$ production cross section, $\sigma_{t\bar{t}}$, is determined as a function of M_t from the number of events observed in each of the counting experiments. Thus, for a given channel,

$$\sigma_{t\bar{t}} = \frac{N_{obs} - B}{A\,\mathcal{L}}, \tag{20}$$

where N_{obs} is the number of observed events, B is the number of expected background events, A is the total acceptance, and $\mathcal{L}$ is the integrated luminosity.

The DØ collaboration uses the results from each of its seven searches to obtain independent measures of the cross section and then combines the results to obtain the best estimate of $\sigma_{t\bar{t}}$. The results from the 50 pb^{-1} analysis is given as a function of M_t in reference [6]. The preliminary result from the 100 pb^{-1} data set is shown in Figure 18 compared with the predicted QCD cross section. Unlike the earlier results, which showed a significant mass dependence, the new results have only a weak dependence on M_t over a large mass range [52].

The corresponding measurement from the CDF collaboration is based on the combination of the cross sections from its dilepton and two lepton + jets searches. The preliminary cross section based on 110 pb^{-1} of data is $7.5\ ^{+1.9}_{-1.6}$ pb [51] for the fitted top quark mass of 176 GeV/c^2 (Section 5.3). This is shown with the DØ results in Figure 18 and in Table 13. The two experimental measurements are consistent with one another and with the predictions of QCD [38-40]. However, because of the present large experimental uncertainties, a more definitive test of the QCD calculations will have to wait for substantially more data.

5.2 *Top Quark Decays*

The Standard Model predicts that the top quark will decay to a W boson and a b-quark almost 100% of the time. The ratio of branching fractions, B($t \rightarrow Wb$)/B($t \rightarrow Wq$), can be measured from the ratio of zero b-tagged to single b-tagged events and the ratio of single b-tagged to double b-tagged events. If a substantial number of top quarks decay to a W boson and a quark other than a b, a deficit of double (single) tags would be observed relative to single (non tagged) events. CDF has measured B($t \rightarrow Wb$)/B($t \rightarrow Wq$) to be 0.94 ± 0.27 (stat) $\pm$ 0.13 (syst) [56]. The CKM matrix element V_{tb} can be determined from B($t \rightarrow Wb$). Assuming that there are three generations and a unitary CKM matrix gives $|V_{tb}| = 0.97 \pm 0.15 \pm 0.07$ while relaxing the three generation assumption gives a lower limit of $|V_{tb}| > 0.022$ at the 95% CL.

A comparison of the cross sections from the different decay channels can reveal anomalies in the decay of the top quark. For instance, the presence of charged Higgs bosons would elevate the lepton + jets cross section relative to the dilepton cross section

$$R = \frac{\sigma_{t\bar{t}}^{\text{lepton+jets}}}{\sigma_{t\bar{t}}^{\text{dilepton}}} \approx 1 + \frac{3}{2}\text{B}(t \rightarrow H^+ b). \qquad (21)$$

Here, the $\sigma_{t\bar{t}}^{\text{lepton+jets}}$ and $\sigma_{t\bar{t}}^{\text{dilepton}}$ are corrected for their relative branching ratios, and B ($t \to H^+b$) is the branching fraction for decay $t \to H^+b$. The present measurements are consistent with the Standard Model expectation of 1 for both experiments (see Table 13). The combined preliminary results give a value of $R = 0.99 \pm 0.52$ where the error is dominated by the statistical uncertainty on $\sigma_{t\bar{t}}^{\text{dilepton}}$.

In the Standard Model, the top quark has rare decay modes such as $t \to \gamma\ q$, $t \to Z\ q$, or even $t \to ZWb$ close to threshold. These decays only occur through loop diagrams so that the branching fractions are extremely small (10^{-7} - 10^{-12}). Any observation of these decays would represent an enormous deviation from the Standard Model. The CDF collaboration has searched for the flavor changing neutral current modes, $t \to \gamma(Z)\ q$ ($q = u, c$). These decay channels use different event samples than the standard top quark analyses. Typically, the events are selected by the presence of a photon or $Z \to \ell\ell$, along with evidence of a W and jets [56]. The γ-decay mode has a much larger acceptance than the Z decay channel because the branching fraction for $Z \to \ell\ell$ is only a few percent. Preliminary measurements indicate the branching fraction to $\gamma\ q$ and $Z\ q$ are less than 2.9% (95% CL) and 90% (90% CL), respectively.

5.3 *Mass Measurements*

Both CDF and DØ have made several determinations of the top quark mass using a variety of fitting techniques and data samples. The most precise of these is based on a two-constraint fit, which reconstructs the t and $\bar{t}$ in a subset of the lepton + jet events having four or more reconstructed hadronic jets.

The fit constrains the invariant mass of the primary lepton and the missing transverse energy to the measured W mass, providing a determination of the neutrino's longitudinal momentum up to a two-fold ambiguity. Next, two jets are selected as coming from the hadronic W decay, and their invariant mass is constrained to the W mass. Lastly, the two W + jet systems, which represent the t and $\bar{t}$ quarks, are constrained to have equal mass. In the absence of tagged b-quark jets there are a total of 24 possible configurations per event (12 from the jet assignments $\times$ 2 from the neutrino ambiguity). If one or more jets have been tagged, these are assigned to either the b or $\bar{b}$ thereby reducing the combinatorics. For each combination, a χ^2 is formed based on the constraints and the goodness of the fit. To determine the best estimate

of the top mass in an event, CDF selects the lowest χ^2 configuration. DØ uses the same technique unless an event has several solutions with similar values of χ^2, in which case a χ^2-weighted average of up to three solutions is used. Events are rejected if no configuration provides a minimally good fit. When the top mass for each event has been determined, the distribution of M_t is fit to a combination of the background (W + jets and QCD multijets) and $t\bar{t}$ distributions. The best estimate of M_t is then extracted by a maximum likelihood technique [42, 44].

The result of the CDF analysis is shown in Figure 19 for the CDF 67 pb^{-1} data sample [5]. The fitted mass is

$$M_t = 176 \pm 8 \text{ (stat)} \pm 10 \text{ (syst) GeV/c}^2, \tag{22}$$

where the first error is the statistical uncertainty from the fit and the second is the systematic uncertainty. The latter includes contributions from the knowledge of the background distribution, the detector energy scale, and biases associated with jet energy corrections, b tagging, and Monte Carlo simulation of top production. For a detailed discussion of these effects, we refer the reader to Reference [44].

Figure 20 shows the mass distributions and fit curves obtained by DØ for both the standard and loose section cuts with the 50 pb^{-1} data sample [6] (see Section 4.2). Independent fits to the two distributions give the same result for M_t. From the loose selection analysis, DØ determines the top quark mass to be

$$M_t = 199 \, ^{+19}_{-21} \text{ (stat)} \, ^{+14}_{-21} \text{ (syst) GeV/c}^2, \tag{23}$$

consistent with the CDF measurement discussed above. For a full discussion of the uncertainties and the error analysis, we refer the reader to Reference [42].

The DØ collaboration has also presented an independent measurement based on the analysis of their dilepton events. Because of the additional ambiguities introduced by the two neutrinos, a different fitting technique is needed. DØ has used an extension of the dynamical fitting techniques discussed in Reference [57] to solve for M_t [58]. From a preliminary analysis they obtain a result of

$$M_t = 145 \pm 25 \text{ (stat)} \pm 20 \text{ (syst) GeV/c}^2, \tag{24}$$

which is consistent, within the large errors, with the lepton + jet determinations. CDF is using an alternate technique for their dilepton events, which uses the shape E_T spectrum of the b-quark jets to measure M_t. Results from this analysis are expected soon.

Several other mass analyses are in progress, and results based on the full CDF and DØ data samples are expected in the near future. These include fits to the all-jets channel (CDF,DØ) using constrained fitting techniques, unconstrained M_t - M_W fits (DØ) [59], and a shape analysis of the $\mathcal{H}$ distribution (CDF) [55].

5.4 *Additional Measurements*

The study of the kinematics of top quark production and decay has just begun. To date, primarily because of the limited statistics, no strong conclusions can be drawn other than the data are consistent with Standard Model predictions in all of the variables investigated. These include the kinematics of the $t\bar{t}$ system (rapidity, mass, P_T, aplanarity), the W (hadronic mass, P_T), the b-quarks (P_T) and the leptons (P_T, angular distribution) [59, 60]. No significant discrepancies have been observed and more data are needed to put these studies on a firmer footing.

5.5 *Summary*

The existence of the top quark has been experimentally verified and the focus of the future research will be the study of top quark properties. Measurements from the early data have established the top quark as the most massive fundamental particle known to science. Its production cross section and principal decay modes appear to be consistent with Standard Model predictions. Refinement of these measurements and a more complete understanding of its production and decay properties will have to wait for larger data samples. The exploration of the top quark sector of the Standard Model has just begun.

6 FUTURE OUTLOOK

The results from the current experiments have focused on the experimental observation of the top quark. The data are statistically limited and allow only a first examination of its production and decay properties. At the time of writing, the current Tevatron run is approaching completion and no further data-taking is planned until 1999. For the

next collider run (Run II), both the accelerator and the detectors will undergo substantial upgrades, which will allow the extension of the current studies of top quark production.

For Run II the Tevatron will undergo both energy and luminosity upgrades. The accelerator is expected to reach an instantaneous luminosity of $\sim 2 \times 10^{32}$ and operate at a center-of-mass energy of 2.0 TeV. Although the machine energy is increasing by only 10%, the $t\bar{t}$ cross section grows by 40%. The tracking systems in both detectors will be completely replaced to utilize the increased instantaneous luminosity [62, 61]. Key elements of the detector upgrades will be the addition of long (~100 cm) silicon-microstrip vertex detectors to provide precision three dimensional tracking and secondary vertex reconstruction. In addition, DØ will add a 2 T solenoidal magnetic field for charged particle momentum analysis.

Projections for Run II show integrated luminosities of in excess of 1 fb^{-1} delivered to both detectors with the prospect of up to $\sim$ 10 fb^{-1} following additional upgrades to the accelerator complex. This will enable the first precise measurements of top quark production and decay, including the ability to set limits on rare decay modes such as $t \rightarrow c+\gamma$ and $t \rightarrow u+\gamma$. Table 14 summarizes the estimated precision on selected quantities for datasets of 1 and 10 fb^{-1} . These are values for a single experiment and are calculated assuming the theoretical cross section for a top quark mass of 175 GeV/c^2. The efficiencies used are extrapolations from the 1994-1995 run values. For a more detailed discussion of top quark physics with high luminosities we refer the reader to Reference [63].

6.1 *Constraints on the Higgs Boson Mass*

In the absence of the physics beyond the Standard Model, the top mass measurement will arguably be the most important of the Run II measurements. With an estimated uncertainty of 3.5 (2.0) GeV/c^2 for 1 (10) fb^{-1} of data (see Table 14), it should be possible to use the relationship between M_t and M_W (see Figure 21) to exclude very large values of the Higgs boson mass, M_H. As such, the Tevatron measurements are complimentary to the Higgs limits accessible to the upgraded CERN e^+e^- collider (LEP200). Alternatively, if the Higgs is observed, the Standard Model becomes over-constrained and the measurements can be used to check for self-consistency.

6.2 *Rare Top Quark Decays*

The limits on the rare decays of the top quark will benefit from the increased data samples. In addition, the branching fraction of the top to longitudinally polarized W bosons ($t \rightarrow W_0 + b$) can be measured from the angular distribution of the leptons in lepton + jet events. The Standard Model predicts this branching fraction to be ~70% for a top mass of 175 GeV/c^2. Deviations from the predicted branching fraction could indicate anomalous couplings at the t-decay vertex. The current data samples are too statistically limited for a meaningful measure of this quantity; however, with 1 (10) fb^{-1} the branching fraction will be measured to a statistical precision of 4.6% (1.5%) [63].

6.3 *Single Top Quark Production*

The primary focus of this article has been the top discovery and the study of $t\bar{t}$ pair production. Studies of single top quark production (see Section 2.3) require high luminosity because of the small cross section (~ 1-2 pb) and large experimental backgrounds. Initial studies will be based on the Run I data but this type of analysis is much better suited to the large data samples expected from Run II.

Single top production is important because it provides access to quantities such as the top quark decay width, Γ_t, which cannot be measured via $t\bar{t}$ pair production. The decay width is proportional to the single top production cross section, σ_{tb}. From estimates of the measurement precision on σ_{tb} for $M_t \sim 180$ GeV/c^2, a measurement of Γ_t to a precision of 10% should be possible [63, 64]. If there are no anomalous couplings to the top quark, this can be turned into a measure of $|V_{tb}|$ with a precision of ~ 4%. This is complimentary to the measurement using B($t \rightarrow Wb$) which places a lower limit on $|V_{tb}|$ but does not provide a good measure unless assumptions are made about unitary constraints and the number of generations in the CKM matrix [56].

7 SUMMARY

In this report we have presented a summary of the present knowledge of the top quark. After 18 years of experimental searches, convincing proof of its existence was finally reported during 1995. As the most

massive fundamental particle known to physics, many questions about its properties remain to be answered. We have summarized the results of the discovery analyses and the first tentative studies of its properties. These studies are still in their infancy, and many new and interesting puzzles remain to be studied in years to come.

ACKNOWLEDGMENTS

The results presented here are the work of the CDF and DØ collaborations at Fermilab. We thank all our colleagues who contributed to the success of this research and to the Fermilab Accelerator, Computing and Research Divisions for their support.

We would also like to thank Jim Cochran, Ann Heinson, Richard Hughes, Robert Roser, Paul Tipton and the TeV2000 Top Working Group for helpful discussions during the preparation of this review. Thanks are also due to the National Science Foundation and the US Department of Energy for their support during the preparation of this review.

References

[1] Glashow S.L., *Nucl. Phys.* B22 : 579 (1968); Weinberg S., *Phys. Rev. Lett.* 19 : 1264 (1967); Salam A., in *Elementary Particle Theory : Relativistic Groups and Analyticity (Nobel Symposium No.8)*, ed. Svartholm N., Almquist and Wiksell Publ., (1968).

[2] Glashow S.L., Illiopoulos J., Maiani L., *Phys. Rev.* D2 : 1285 (1970); Kobayashi M., Maskawa M., *Prog. Theor. Phys.* 49 : 652 (1973).

[3] Perl M.L. et al, *Phys. Lett.* 70B : 487 (1977).

[4] Herb S.E. et al, *Phys. Rev. Lett.* 39 : 252 (1977).

[5] Abe F. et al (CDF Collaboration). *Phys. Rev. Lett.* 74 : 2626 (1995).

[6] Abachi S. et al (DØ Collaboration), *Phys. Rev. Lett.* 74 : 2632 (1995).

[7] Marshall R., *Zeit. Phys.* C43 : 607 (1989); Wu S.L., in *1987 Int. Symp. on Lepton and Photon Interactions at High Energies* , Hamburg, North Holland Publ., (1988).

[8] Barger V. and Pakvasa S., *Phys. Lett.* 81B : 195 (1979); Kane G.L. and Peskin M.E., *Nucl. Phys.* B195 : 29 (1982); Deshpande N.G., Eilam G., Soni A. and Kane G.L., *Phys. Rev. Lett.* 56 : 1106 (1986).

[9] Bean A. et al (CLEO Collaboration), *Phys. Rev.* D35 : 3533 (1987).

[10] Roy D.P. and Sankar U., *Phys. Lett.* 243B : 296 (1990).

[11] Albrecht H. et al (ARGUS Collaboration), *Phys. Lett.* 192B : 245 (1987); *Zeit. Phys.* C55 : 357 (1992); *Phys. Lett.* B324 :249 (1994); Artuso M. et al (CLEO Collaboration), *Phys. Rev. Lett.* 62 : 2233 (1989); Bartelt J. et al (CLEO Collaboration), *Phys. Rev. Lett.* 71 : 1680 (1993).

[12] The LEP Collaborations and the LEP Electroweak Working Group, CERN- PPE/94-187; Schaille D. In *XXVII th Int. Conf. on High Energy Physics*, Glasgow, IOP Publ., (1995).

[13] Forty R., in *XXVII th Int. Conf. on High Energy Physics*, Glasgow, IOP Publ. (1995).

[14] Franzini P., *Phys. Rep.* 173 : 1 (1989) and references contained therein.

[15] Albajar C. et al (UA1 Collaboration), *Zeit. Phys.* C44 : 15 (1989); Abe F. et al (CDF Collaboration) *Phys. Rev. Lett.* 74, 341, (1995).

[16] Cabibbo N., in *3rd Topical Workshop on Proton-Antiproton Collider Physics*, Rome, CERN Report No. CERN 83-04 : 567 (1983); Halzen F. and Mursula K., *Phys. Rev. Lett.* 51 : 857 (1983).

[17] Abe F. et al (CDF Collaboration), *Phys. Rev. Lett.* 73 : 220 (1994); *Phys. Rev. Lett.* 74 : 341 (1995); Abachi S. et al (DØ Collaboration), *Phys. Rev. Lett.* 75 : 1456 (1995).

[18] Rosner J.L., Worah M.P. and Takeuchi T., *Phys. Rev.* D49 : 1363 (1994).

[19] Marciano W.J. and Sirlin A., *Phys. Rev.* D29 : 945 (1984).

[20] Marciano W.J., *Phys. Rev.* D20 : 945 (1984); Sirlin A., *Phys. Rev.* D22 : 971 (1980).

[21] Antonelli F. et al, *Phys. Lett.* 91B : 90 (1980); Veltman M., *Phys. Lett.* 91B : 95 (1980).

[22] Djouadi A. and Verzegnassi C., *Phys. Lett.* B195 : 265 (1987); Kniehl B.A., Kuhn J.H. and Stuart R.G., *Phys. Lett.* B214 : 621 (1988); Halzen F. and Kniehl B.Z., *Nucl. Phys.* B353 : 567 (1991).

[23] Amaldi U. et al, *Phys. Rev.* D36 : 1385 (1987); Costa G. et al, *Nucl. Phys.* B297: 244 (1988); Ellis J. and Fogli G., *Phys. Lett.* B213 : 526 (1988); *Phys. Lett.* B231: 189 (1989); *Phys. Lett.* 232B : 139 (1989); Langacker P., *Phys. Rev. Lett.* 63 : 1920 (1989).

[24] Ellis J. and Fogli G.L, *Phys. Lett.*B249 : 543 (1990); Ellis J., Fogli G.L. and Lisi E., *Phys. Lett.* B274 : 456 (1992); *Phys. Lett.* B292 : 427 (1992); *Phys. Lett.* B333 : 118 (1994); del Agulila F.L., Hollik W.F.L., Moreno J.M. and Quiros M., *Nucl. Phys.* B372 : 3 (1992); del Agulila F.L., Martinez M. and Quiros M., *Nucl. Phys.* B381 : 451 (1992); Novikov V.A., Okun L.B., Vyotskii M.I. and Yurov V.P., *Phys. Lett.* B308 : 123 (1993); Novikov V.A., Okun L.B., Rozanov A.N., Vyotskii M.I. and Yurov V.P., *Phys. Lett.* B331 : 433 (1994).

[25] Langacker P. and Luo M., *Phys. Rev.* D44 : 817 (1991); Erler J. and Langacker P., *Phys. Rev.* D52 : 441 (1995); Passarino G., *Phys. Lett.* B255 : 127 (1991); Montagna G., Nicrosini O., Passorino G. and Piccinini F., *Phys. Lett.* B335 : 484 (1994); Altarelli G., Barbieri R. and Caravaglios F., *Nucl. Phys.* B405 : 3 (1994); Banerjee S., Ganguli S.N. and Gurtu A., *Int. J. Mod. Phys.* A7 : 1853 (1992); Gonzalez M.C. and Valle J.W.F., *Phys. Lett.* B259 : 365 (1991); Schaille D., *Fortschr. Phys.* 429 : 429 (1994).

[26] Buskulic D. et al (ALEPH Collaboration), *Phys. Lett.* B313 : 299 (1993); Abreu P. et al (DELPHI Collaboration), *Nucl. Phys.* B421 : 3 (1994); Adriani O. et al (L3 Collaboration), *Phys. Lett.* B303 : 391 (1993); Akers R. et al (OPAL Collaboration), *Phys. Lett.* B327 : 397 (1994).

[27] Ellis J., Fogli G.L. and Lisi E., CERN Report No. CERN-TH/95-202 (1995).

[28] Chankowski P.H. and Pokorski S., Max Planck Institute Report No. MPI-Ph/95-39 (1995).

[29] Eno S. et al (AMY Collaboration), *Phys. Rev. Lett.* 63 : 1910 (1989); Adachi I. et al (TOPAZ Collaboration), *Phys. Lett.* B234 : 525 (1990); Abe K. et al (VENUS Collaboration), *Phys. Lett.* B234 : 382 (1990).

[30] Abrams G.S. et al (Mark 2 Collaboration), *Phys. Rev. Lett.* 63 : 2447 (1989).

[31] Decamp D. et al (ALEPH Collaboration), *Phys. Lett.* B236 : 511 (1990); Abreu P. et al (DELPHI Collaboration), *Phys. Lett.* B242 : 536 (1990); Akrawy M.Z. et al (OPAL Collaboration), *Phys. Lett.* B236 : 364 (1990); Adriani O. et al (L3 Collaboration), *Phys. Lett.* B313 : 326 (1993).

[32] Nason P., Dawson S. and Ellis R.K., *Nucl. Phys.* B303 : 607 (1988); *Nucl. Phys.* B327 : 49 (1989).

[33] Altarelli G.,Diemoz M., Martinelli G. and Nason P., *Nucl. Phys.* B308 : 724 (1988).

[34] Beenaker W., Kuijf H., Van Neervan W.L. and Smith J., *Phys. Rev.* D40 : 54 (1989); Meng R., Schuler G.A., Smith J. and Van Neervan W.L., *Nucl. Phys.* B339 : 325 (1990); Beenaker W., Van Neervan

W.L., Meng R., Schuler G.A. and Smith J., *Nucl. Phys.* B351 : 507 (1991).

[35] Albajar C. et al (UA1 Collaboration), *Zeit. Phys.* C48 : 1 (1990); Akesson T. et al (UA2 Collaboration), *Zeit. Phys.* C46 : 179 (1990).

[36] Abe. F. et al (CDF Collaboration), *Phys. Rev. Lett.* 68 : 447 (1992); *Phys. Rev.* D45 : 3921 (1992).

[37] Ellis R.K., *Phys. Lett.* B259 : 492 (1991).

[38] Laenen E., Smith J. and van Neervan W., *Phys. Lett.* B321 : 254 (1994); *Nucl. Phys.* B369 : 543 (1992).

[39] Berger E. and Contapanagos J., Argonne Preprint No. ANL-HEP-CP-95-85, submitted for publication.

[40] Cantini S., Mangano M., Nason P. and Trentadue L., CERN Preprint No. CERN-TH-96/21, January, (1996).

[41] Abachi S. et al (DØ Collaboration), *Phys. Rev. Lett.* 72 : 2138 (1995).

[42] Abachi S. et al (DØ Collaboration), *Phys. Rev.* D52 : 4877 (1995).

[43] Abachi S. et al (DØ Collaboration), *Phys. Rev. Lett.* 74 : 2422 (1995).

[44] Abe F. et al (CDF Collaboration), *Phys. Rev. Lett.* 73 : 225 (1994); *Phys. Rev.* D50 : 2966 (1994).

[45] Bordes G. and van Eijk B..*Nucl. Phys.* B435 : 23 (1995), *Zeit. Phys.* C57 : 81 (1993); Carlson D.O. and Yuan C.-P., *Phys. Lett.* B306 : 386 (1993), Michigan State Preprint, MSUHEP-50823, (August 1995); Cortese S. and Petronzio R., *Phys. Lett.* B253 : 494 (1991); Dawson S., *Nucl. Phys.* B249 : 42 (1995); Ellis, R.K. and Parke S., *Phys. Rev.* D46 : 3785 (1992); Moers T., Priem R., Rein. D. and Reitler H., in *Proceedings of the Large Hadron Collider Workshop*, Aachen, (1990); Steltzer T. and Willenbrock S., *Phys. Lett.* B357 : 125 (1995); Willenbrock S.S.D. and Dicus D.A., *Phys. Rev.* D34 : 155 (1986).

[46] C.-P. Yuan, *Phys. Rev.*D41 : 42 (1990); Jikia G.V. and Slabospitsky S.R., *Phys. Lett.* B295 : 136 (1992); Carlson D.O., Malkawi E. and Yuan C.-P., *Phys. Lett.* B337 : 145 (1994); Malkavi E. and Yuan

C.-P.,*Phys. Rev.* D50 : 4462 (1994); Yuan C.-P., *Mod. Phys. Lett.* A10 : 627 (1995); Belayev A.S., Boos E.E. and Heinson A.P., in *Proceedings of Workshop on the Top Quark*, IITAP, Iowa State University, May (1995); manuscript in preparation.

[47] Thompson J., Fermilab TM/1909, (1994), (and references contained therein).

[48] Abachi S. et al (DØ Collaboration), *Nucl. Instrum. Methods* A338 : 185 (1995).

[49] Abe F. et al (CDF Collaboration), *Nucl. Instrum. Methods* A271 : 387 (1988).

[50] Azzi P. et al (CDF Collaboration), Fermilab-Conf-94/205-E, (1994); Amidei D. et al (CDF Collaboration), *Nucl. Instrum. Methods* A350 : 73 (1994).

[51] Caner A. (CDF Collaboration), in *Les Recontres de Physique de la Vallee d'Aosta*, La Thuile, Italy, February 1996; Azzi. P. (CDF Collaboration), in *Recontres de Moriond*, Moriond, France, March 1996.

[52] Li-Demarteau Q. (DØ Collaboration), in *1996 Aspen Winter Physics Conference on Particle Physics*, January 1996; Narain M. (DØ Collaboration), in *Les Recontres de Physique de la Vallee d'Aosta*, La Thuile, Italy, February 1996.

[53] Giele W., Glover E. and Kosower D., *Nucl. Phys.* B403 : 633 (1993).

[54] Abe F. et al (CDF Collaboration), *Phys. Rev. D. Rapid Communications*, 52, R2605 (1995).

[55] Abe F. et al (CDF Collaboration), *Phys. Rev. Lett.* 75, 3997 (1995).

[56] LeCompte T. (CDF Collaboration), in *Reconres du Vietnam*, Ho Chi Minh City, Vietnam, October 1995.

[57] Kondo K., *J. Phys. Soc. Japan* 57 : 4126 (1988), *J. Phys. Soc. Japan* 60 : 836 (1991); Dalitz R.H. and Goldstein G.R., *Phys. Rev.* D45 : 1531 (1992).

[58] Cochran J. (DØ Collaboration), in *Conference on the Production and Decay of Hyperons. Charm and Beauty Hadrons*, Strasbourg, (1995).

[59] Snyder S. (DØ Collaboration), in *International Europhysics Conference on High Energy Physics (HEP 95)*, Brussels, (1995).

[60] Beretvas, A. (CDF Collaboration), Fermilab-Pub-95/311, to appear in *Int. J. Mod. Phys.*, (1995).

[61] Abachi S. et al (DØ Collaboration), *The DØ Upgrade*, Fermilab-Conf-95/177, (1995).

[62] CDF Collaboration. *The CDF Upgrade Proposal*, CDF Note 3171, (1995).

[63] Amidei D., Brock R. eds. In *Report of the Tev 2000 Study Group on Future Electroweak Physics at the Tevatron*, DØ note 2589, CDF note 3177, (1996).

[64] Baringer P. and Heinson A.P., *Single Top Physics with a High Luminosity Tevatron*, DØ note 2600, (1995).

Figure Captions

Figure 1: Lowest-order Feynman diagrams for $t\bar{t}$ pair production : (a) $q\bar{q} \rightarrow t\bar{t}$; and (b) $gg \rightarrow t\bar{t}$.

Figure 2: The total cross section for the production of $t\bar{t}$ pairs in $p\bar{p}$ collisions at 1.8 TeV. Two different calculations are shown, corresponding to the results from References 38 and 39.

Figure 3: The DØ 95 % CL limit on $\sigma_{t\bar{t}}$ as a function of M_t [41]. Also shown are the range of QCD predictions for the cross section from reference 38.

Figure 4: The measured $t\bar{t}$ production cross section (*solid line*),(shaded region corresponds to the one standard deviation error) as a function of M_t from the DØ high mass study [43]. Also shown are the range of QCD predictions for the cross section from reference [38].

Figure 5: CDF top quark mass distribution for lepton + jet events collected in 1992-1993. (*Solid histogram*) data; (*dashed histogram*) combined fit to $t\bar{t}$ and background (*dotted*) distributions.

Figure 6: Schematic of the Tevatron Collider complex at Fermi National Accelerator Laboratory.

Figure 7: Schematic cross section of one quarter of the Collider Detector at Fermilab. The detector is cylindrically and forward-backward symmetric.

Figure 8: A cut-away isometric view of the DØ detector.

Figure 9: A $t\bar{t} \rightarrow \mu^+\nu b e^-\bar{\nu}\bar{b}$ candidate from the DØ dilepton analysis. Shown in outline are side views of the central tracking system and calorimeters. The solid lines coming from the interaction point represent the trajectories of charged particles in the detector and the boxes drawn on the calorimeter indicate energy deposition in the calorimeter cells.

Figure 10: Comparison of the jet multiplicity distribution for data and $t\bar{t}$ Monte Carlo after tight W and jet selection cuts have been applied. The points are data from the DØ experiment and the shaded bands are the expectation for $t\bar{t}$ production for $M_t = 180$ GeV/c^2.

Figure 11: Lepton + jets events from the DØ experiment : Number of events with $b \rightarrow \mu$ tags (*squares*), and the expected number of background events (*circles*) versus jet multiplicity.

Figure 12: Charged-particle tracks (*solid lines*) reconstructed in the CDF silicon vertex detector. The primary vertex is the $p\bar{p}$ interaction point. L_{xy} is the two-dimensional decay distance to the secondary vertex, and d is the minimum distance of approach of tracks from the secondary vertex when projected to the primary vertex position.

Figure 13: CDF Experiment : Number of events before displaced vertex tagging (*circles*), number of tags observed (*triangles*), and the expected number of background tags (*dashed*) versus jet multiplicity. The shaded areas indicate the expectation for background plus a $t\bar{t}$ contribution.

Figure 14: A CDF lepton + jet $t\bar{t}$ candidate shown as a closeup of the interaction point. The lines emerging from the vertices are charged tracks measured by the silicon vertex detector. The jets are reconstucted in the calorimeter (not shown) and are labeled 1-4. Jet 1 and 4 each exhibit a secondary vertex clearly displaced from the primary vertex. Jets 2 and 4, mostly likely the $W \rightarrow q\bar{q}$ decay, have an invariant mass of 79 GeV/c^2.

Figure 15: H_T distributions for (a) $W + \geq 2$ jets and (b) $W + \geq 3$ jet events. The points are DØ data and the curves are the predicted spectra calculated using the Vecbos Monte Carlo.

Figure 16: The CDF kinematic relative likelihood distribution, $\ln(\mathcal{L})$. Events with $\ln(\mathcal{L}) > 0$ are more top-like and those with $\ln(\mathcal{L}) < 0$ are more background-like.

Figure 17: The CDF $\mathcal{H}$ distribution. A combined fit of background and $t\bar{t}$ is shown, and b-tagged events are shaded.

Figure 18: The $t\bar{t}$ production cross section as a function of the top quark mass. The shaded area shows the preliminary measurement from DØ as a function of M_t. The point is the preliminary result from CDF, plotted at top mass measured from the CDF data [5]. Also shown are the QCD predictions from references 38 and 39.

Figure 19: The reconstructed mass distribution for the CDF b-tagged lepton + $\geq$ 4 jet data: (*solid histogram*) data, (*dotted histogram*) background, and (*dashed histogram*) fit signal + background. The inset distribution is the change in log-likelihood for the fit.

Figure 20: The fitted mass and likelihood distributions from the DØ lepton + jets analyses: (*solid curves*) signal + background, (*dotted curves*) top signal, and (*dashed curves*) background. The shaded histogram indicates the position of the events with a $b \rightarrow \mu$ tag.

Figure 21: Projected future measurements of M_W, and sensitivity to the Higgs Boson mass: M_W vs M_H with a band representing the expected region for a top mass of 175 GeV/c^2 measured to a precision of 2 GeV/c^2. A hypothetical W mass measurement is shown with 20 MeV/c^2 uncertainty and plotted at the current experimental value.

Tables

Table 1: The generations of the Standard Model.

Generation			Electric	Isospin
I	II	III	charge, Q	I_3
Leptons				
ν_e	ν_μ	ν_τ	0	$\frac{1}{2}$
e	μ	τ	-1	$-\frac{1}{2}$
Quarks				
u	c	t	$\frac{2}{3}$	$\frac{1}{2}$
d	s	b	$-\frac{1}{3}$	$-\frac{1}{2}$

Table 2: Definition of the $t\bar{t}$ search channels and the contributing $t\bar{t}$ decays. The symbol $q\bar{q}$ denotes the hadronic decays $W^+ \rightarrow c\bar{s}$ and $W^+ \rightarrow u\bar{d}$ and their charge conjugates. The multiplicative factors correspond to the branching fractions for the appropriate τ decays.

Channel	Contributing decays	Branching fraction
ee	$t\bar{t} \rightarrow e^+\nu_e b e^-\bar{\nu}_e b$	$\frac{1}{81}$
	$t\bar{t} \rightarrow e^+\nu_e b \tau^-\bar{\nu}_\tau \bar{b}, \tau^- \rightarrow e^-\bar{\nu}_e\nu_\tau$	$\frac{2}{81} \times 0.18$
	$t\bar{t} \rightarrow \tau^+\nu_\tau b\ \tau^-\bar{\nu}_\tau\bar{b}$	
	with $\tau^+ \rightarrow e^+\nu_e\bar{\nu}_\tau, \tau^- \rightarrow e^-\bar{\nu}_e\nu_\tau$	$\frac{1}{81} \times (0.18)^2$
$\mu\mu$	$t\bar{t} \rightarrow \mu^+\nu_\mu b \mu^-\bar{\nu}_\mu b$	$\frac{1}{81}$
	$t\bar{t} \rightarrow \mu^+\nu_\mu b \tau^-\bar{\nu}_\tau \bar{b}, \tau^- \rightarrow \mu^-\bar{\nu}_\mu\nu_\tau$	$\frac{2}{81} \times 0.18$
	$t\bar{t} \rightarrow \tau^+\nu_\tau b\ \tau^-\bar{\nu}_\tau\bar{b}$	
	with $\tau^+ \rightarrow \mu^+\nu_\mu\bar{\nu}_\tau, \tau^- \rightarrow \mu^-\bar{\nu}_\mu\nu_\tau$	$\frac{1}{81} \times (0.18)^2$
$e\mu$	$t\bar{t} \rightarrow e^+\nu_e b \mu^-\bar{\nu}_\mu b$	$\frac{2}{81}$
	$t\bar{t} \rightarrow e^+\nu_e b \tau^-\bar{\nu}_\tau \bar{b}, \tau^- \rightarrow \mu^-\bar{\nu}_\mu\nu_\tau$	$\frac{2}{81} \times 0.18$
	$t\bar{t} \rightarrow \mu^+\nu_\mu b \tau^-\bar{\nu}_\tau \bar{b}, \tau^- \rightarrow e^-\bar{\nu}_e\nu_\tau$	$\frac{2}{81} \times 0.18$
	$t\bar{t} \rightarrow \tau^+\nu_\tau b \tau^-\bar{\nu}_\tau\bar{b}$	
	with $\tau^+ \rightarrow e^+\nu_e\bar{\nu}_\tau, \tau^- \rightarrow \mu^-\bar{\nu}_\mu\nu_\tau$	$\frac{1}{81} \times (0.18)^2$
e + jets	$t\bar{t} \rightarrow e^+\nu_e b q\bar{q} b$	$\frac{12}{81}$
	$t\bar{t} \rightarrow \tau^+\nu_e b q\bar{q}\bar{b}, \tau^+ \rightarrow e^+\nu_e\bar{\nu}_\tau$	$\frac{12}{81} \times 0.18$
	$t\bar{t} \rightarrow e^+\nu_e b \tau^-\bar{\nu}_\tau \bar{b}, \tau^- \rightarrow$ hadrons	$\frac{2}{81} \times 0.498$
μ + jets	$t\bar{t} \rightarrow \mu^+\nu_\mu b q\bar{q} b$	$\frac{12}{81}$
	$t\bar{t} \rightarrow \tau^+\nu_e b q\bar{q}\bar{b}, \tau^+ \rightarrow \mu^+\nu_e\bar{\nu}_\tau$	$\frac{12}{81} \times 0.18$
	$t\bar{t} \rightarrow \mu^+\nu_e b \tau^-\bar{\nu}_\tau \bar{b}, \tau^- \rightarrow$ hadrons	$\frac{2}{81} \times 0.498$
all-jets	$t\bar{t} \rightarrow q\bar{q} b q\bar{q} b$	$\frac{36}{81}$

Table 3: Event samples from DØ 1992-1993 high mass analyses.

Search	Channel			Total	Background
dilepton	ee	$\mu\mu$	$e\mu$		
	0	0	1	1	0.76 ± 0.11
lepton + jets	e + jets	μ + jets			
(topological tag)	2	2		4	2.0 ± 0.9
($b \rightarrow \mu$ tag)	2	2		4	1.0 ± 0.2

Table 4: Event samples from CDF 1992-1993 analyses.

Search	Channel			Total	Background
dilepton	ee	$\mu\mu$	$e\mu$		
	0	0	2	2	$0.56^{+0.25}_{-0.13}$
lepton + jets	e+jets	μ+jets			
(displaced vertex tag)	2	4		6	2.3 ± 0.3
($b \rightarrow \ell$ tag)	3	4		7	3.1 ± 0.3

Table 5: CDF dilepton selection cuts

Oppositely charged leptons		Jets		
Lepton 1	Lepton 2	N_{jet}	E_T^{Jet}	$\not\!\!E_T$
$P_T^\ell > 20$ GeV/c	$P_T^\ell > 20$ GeV/c	≥ 2	>10 GeV	> 25 GeV
tight id	loose id	$\lvert\eta\rvert < 2.4$		

Table 6: DØ dilepton selection cuts

	Channel		
Quantity	ee	$\mu\mu$	$e\mu$
P_{T}^{ℓ} (GeV/c)	$> 20/20$	$> 15/15$	$> 15/15$
$\not\!\!E_{\mathrm{T}}$ (GeV)	> 25	-	> 20
$\mathrm{N_{jet}}$	≥ 2	≥ 2	≥ 2
$E_{\mathrm{T}}^{\mathrm{Jet}}$ (GeV)	> 20	> 20	> 20
H_{T} (GeV)	> 120	> 100	> 120

Table 7: Summary of the CDF and DØ dilepton search results. The results quoted in the upper part of the table are from the published analyses (see text) and those in the bottom part of the table are the preliminary results from the full Run I datasets.

Discovery analyses					
Experiment	Number of events				Background
	ee	$\mu\mu$	$e\mu$	Total	
CDF (67 pb^{-1})	0	1	5	6	1.3 ± 0.3
DØ (50 pb^{-1})	0	1	2	3	0.7 ± 0.2
Full Run I analyses (preliminary)					
CDF (110 pb^{-1})	1	2	7	10	2.1 ± 0.4
DØ (100 pb^{-1})	1	1	3	5	1.6 ± 0.3

Table 8: DØ lepton + jets topological selection cuts

	Channel	
Quantity	e + jets	μ + jets
P_{T}^{ℓ} (GeV/c)	> 20	> 20
$\not\!\!E_{\mathrm{T}}$ (GeV)	> 25	> 20
$\mathrm{N_{jet}}$	≥ 4	≥ 4
$E_{\mathrm{T}}^{\mathrm{Jet}}$ (GeV)	> 15	> 15
H_{T} (GeV)	> 200	> 200
$\mathcal{A}$	> 0.05	> 0.05

Table 9: The CDF lepton (e, μ) + jet kinematic selection. The primary lepton is required to pass strict selection criteria.

Quantity	Cut
P_{T}^{ℓ}	> 20 GeV/c
$\not\!\!E_{\mathrm{T}}$	> 20 GeV
$\mathrm{N_{jet}}$	≥ 3
$E_{\mathrm{T}}^{\mathrm{Jet}}$	> 15 GeV
$\lvert\eta_{\mathrm{jet}}\rvert$	< 2.0

Table 10: Summary of the CDF lepton + jets searches. The numbers in the upper part of the table are from the published analyses and those from the lower section are the corresponding preliminary results from the complete Run I dataset.

CDF analyses (67 pb^{-1})		
Search	No. of Tags (Events)	Background
ℓ + jets (displaced vertex tag)	27 (21)	6.7 ± 2.1
ℓ + jets ($b \rightarrow \ell$ tag)	23 (22)	15.4 ± 2.0
Full Run I analyses (preliminary, 110 pb^{-1})		
ℓ + jets (displaced vertex tag)	42 (34)	9.4 ± 1.5
ℓ + jets ($b \rightarrow \ell$ tag)	44 (40)	26.2 ± 3.9

Table 11: Summary of the DØ lepton + jets searches. The numbers in the upper part of the table are from the published analyses and those from the lower section are the corresponding preliminary results from the complete Run I dataset.

DØ analyses (50 pb^{-1})				
	No. of Events			Background
Search	e + jets	μ + jets	Total	
ℓ + jets (topological tag)	5	3	8	1.9 ± 0.4
ℓ + jets ($b \rightarrow \mu$ tag)	3	3	6	1.2 ± 0.2
Full Run I analyses (preliminary, 100 pb^{-1})				
ℓ + jets (topological tag)	10	11	21	9.2 ± 2.8
ℓ + jets ($b \rightarrow \mu$ tag)	5	6	11	2.6 ± 0.6

Table 12: Summary of the results from the published DØ and CDF counting experiments.

Search	No. of Events Data	No. of Events Background	Fluctuation Probability
DØ counting experiments			
dilepton	3	0.7 ± 0.2	3×10^{-2}
lepton + jets (topological tag)	8	1.0 ± 0.4	2×10^{-3}
lepton + jets ($b \rightarrow \mu$ tag)	6	1.2 ± 0.2	2×10^{-3}
CDF counting experiments			
dilepton	6	1.3 ± 0.3	3×10^{-3}
lepton + jets (displaced vertex tag)	27 tags	6.7 ± 2.1	2×10^{-5}
lepton + jets ($b \rightarrow \ell$ tag)	23 tags	15.4 ± 2.3	6×10^{-2}

Table 13: Preliminary measurements of the $t\bar{t}$ production cross section from the CDF and DØ dilepton and lepton + jets searches.

Search	CDF (110 pb^{-1})	DØ (100 pb^{-1})
dilepton	$9.3\ ^{+4.4}_{-3.4}$ pb	4.6 ± 3.1 pb
lepton + jet (topological tag)	-	3.9 ± 1.9 pb
lepton + jet ($b \rightarrow \mu$ tag)	$7.8\ ^{+4.4}_{-3.7}$ pb	6.8 ± 3.2 pb
lepton + jet (displaced vertex tag)	$6.8\ ^{+2.3}_{-1.8}$ pb	-
Combined	$7.5\ ^{+1.9}_{-1.6}$ pb	4.7 ± 1.6 pb

Table 14: Estimated precision of top measurements from Tevatron Run II with integrated luminosities of 1 and 10 fb^{-1} with an upgraded detector.

Measurement	Expected precision	
	1 fb^{-1}	10 fb^{-1}
δM_t	3.5 GeV/c^2	2 GeV/c^2
$\delta\sigma_{t\bar{t}}$	11%	6%
$\delta\sigma_{t\bar{b}}$	19%	10%
$\delta Br(t\bar{t} \to \ell\ell)/Br(t\bar{t} \to \ell + \text{jets})$	14%	4.8%
$\delta Br(t \to Wb)/Br(t \to Wq)$	3.3%	1.0%
$\|V_{tb}\|$, Lower limit	> 0.22	> 0.40
$\delta\|V_{tb}\|$	19%	4%
$Br(t \to W + s(d))$ Limit	$< 7\%$	$< 2\%$
$Br(t \to c(u) + \gamma)$ Limit	$< 0.3\%$	$< 0.04\%$
$Br(t \to c(u) + Z)$ Limit	$< 1.5\%$	$< 0.4\%$
$Br(t \to H + b)$ Limit	$< 15\%$	$< 6\%$
$\delta Br(t \to W_0 + b)$	4.6%	1.5%
$\delta Br(t \to W_+ + b)$	1.9%	0.6%

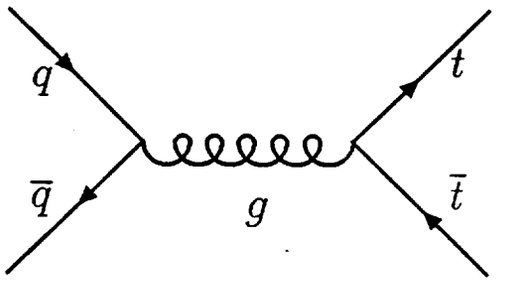

(a)

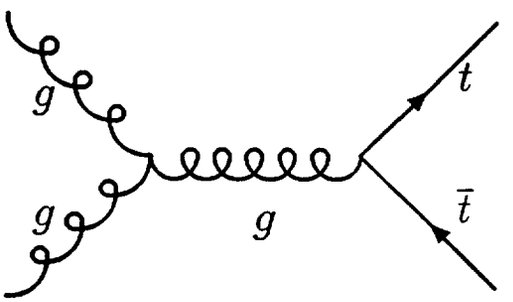

(b)

Wimpenny & Winer Fig. 1

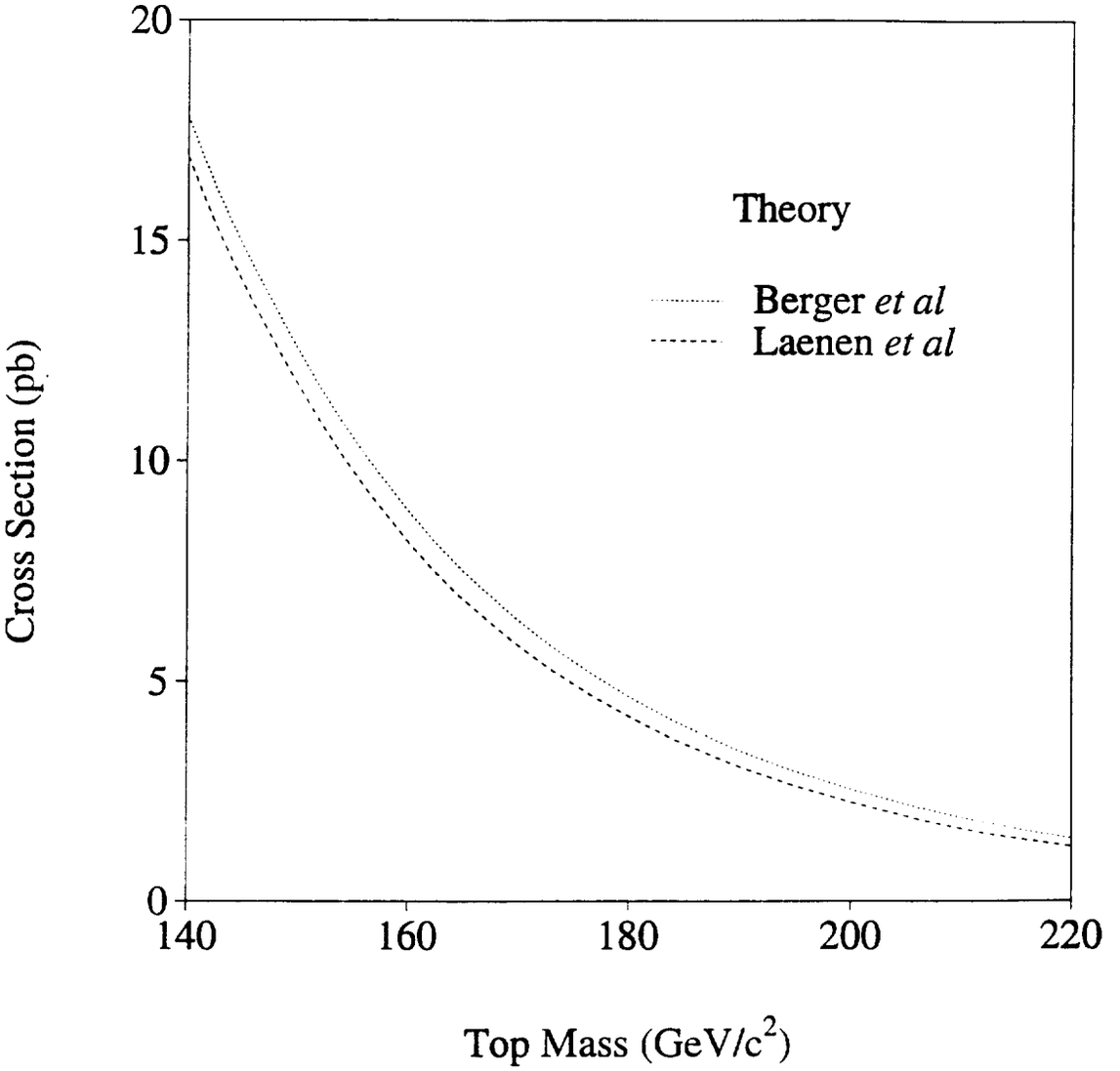

Wimpenny & Winer Fig. 2

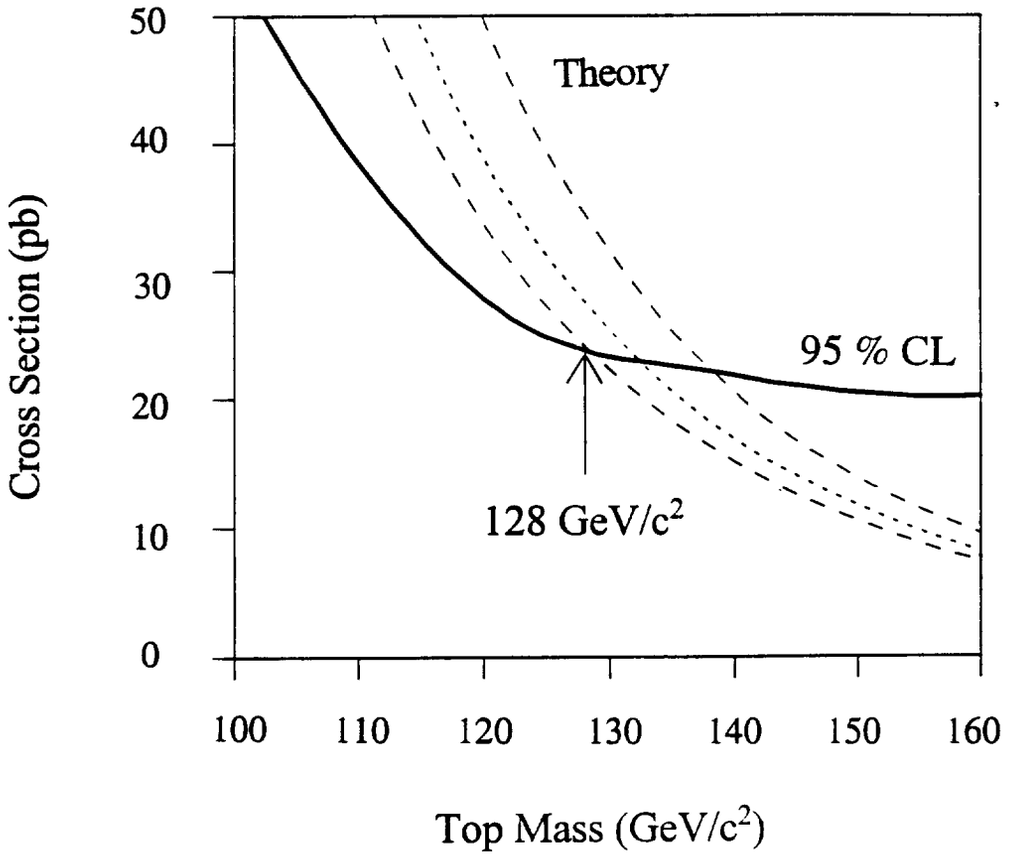

Wimpenny & Winer Fig. 3

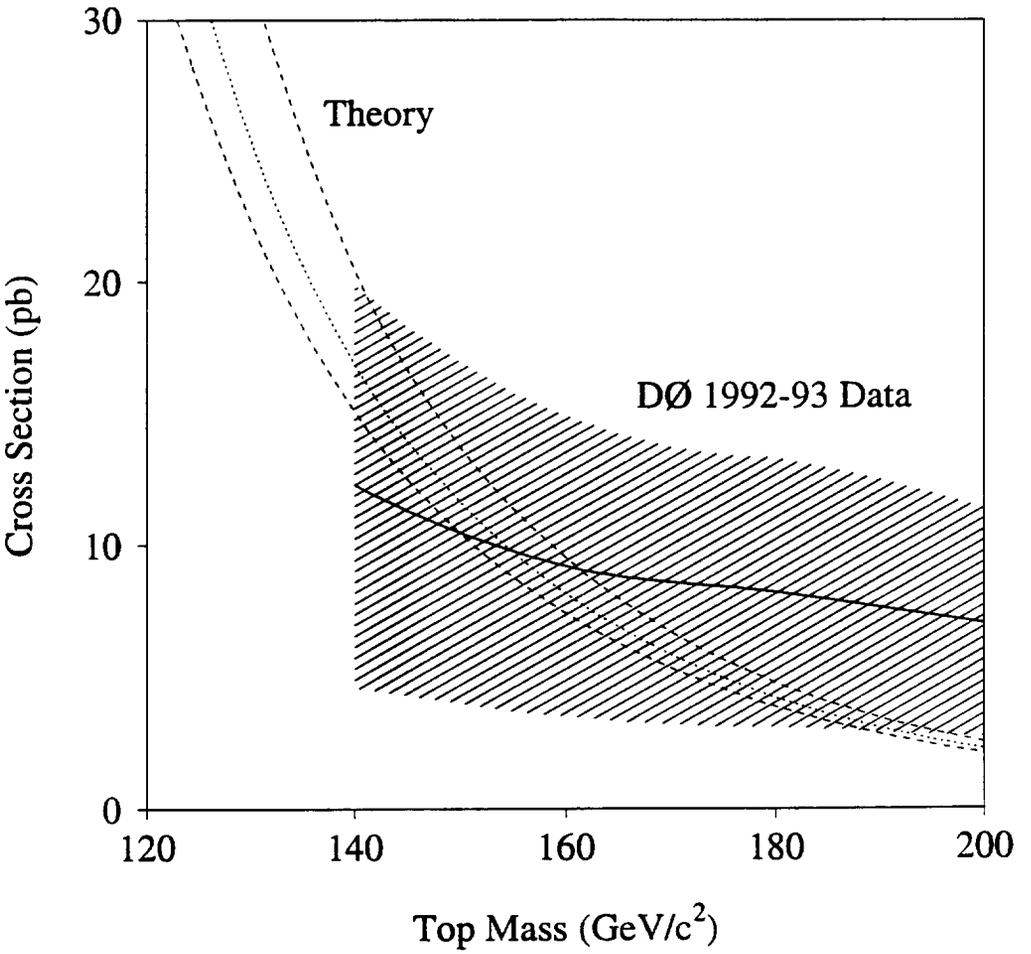

Wimpenny & Winer Fig. 4

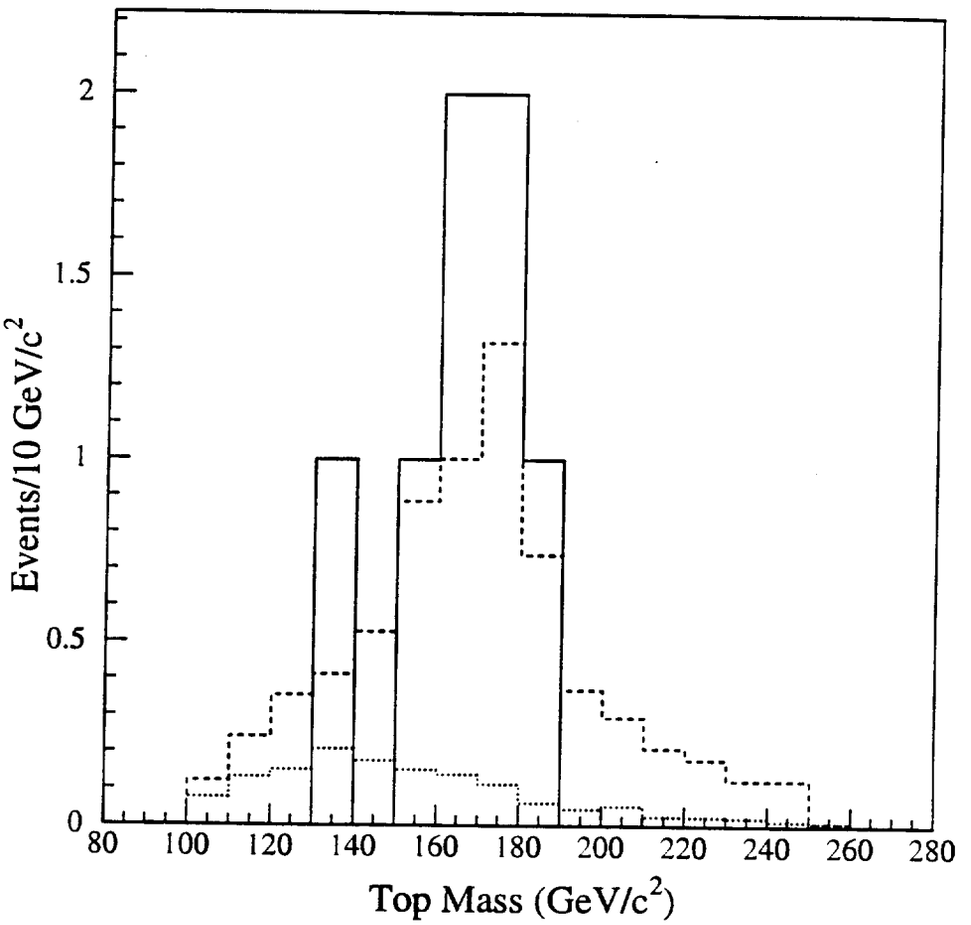

Wimpenny & Winer Fig. 5

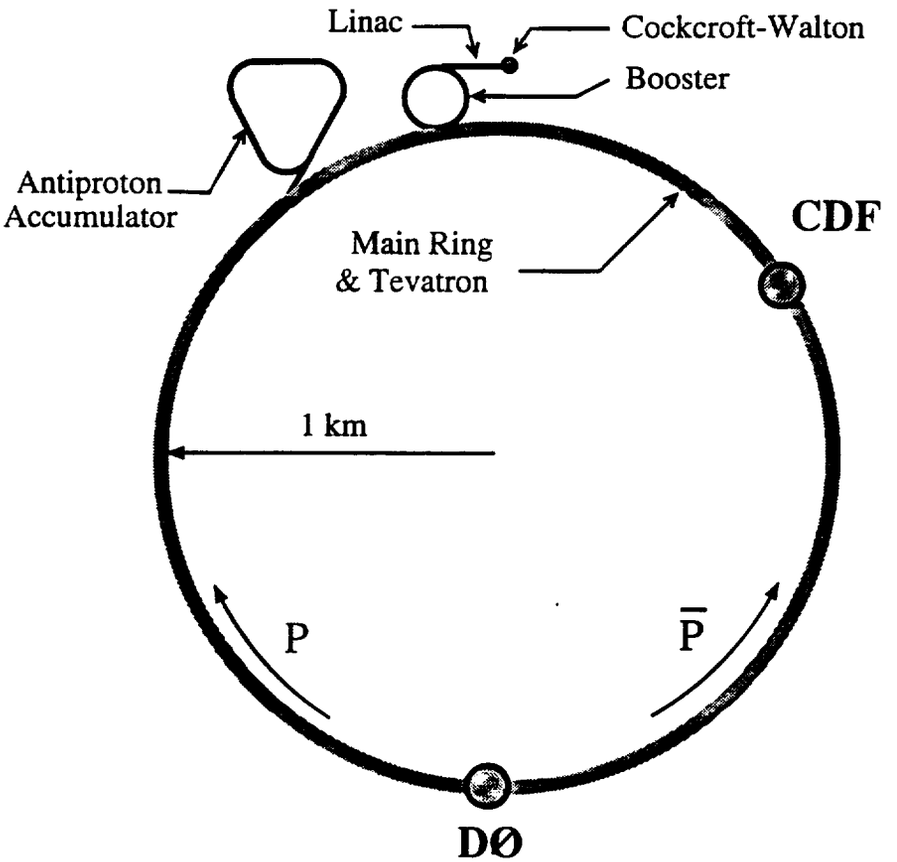

Wimpenny & Winer Fig. 6

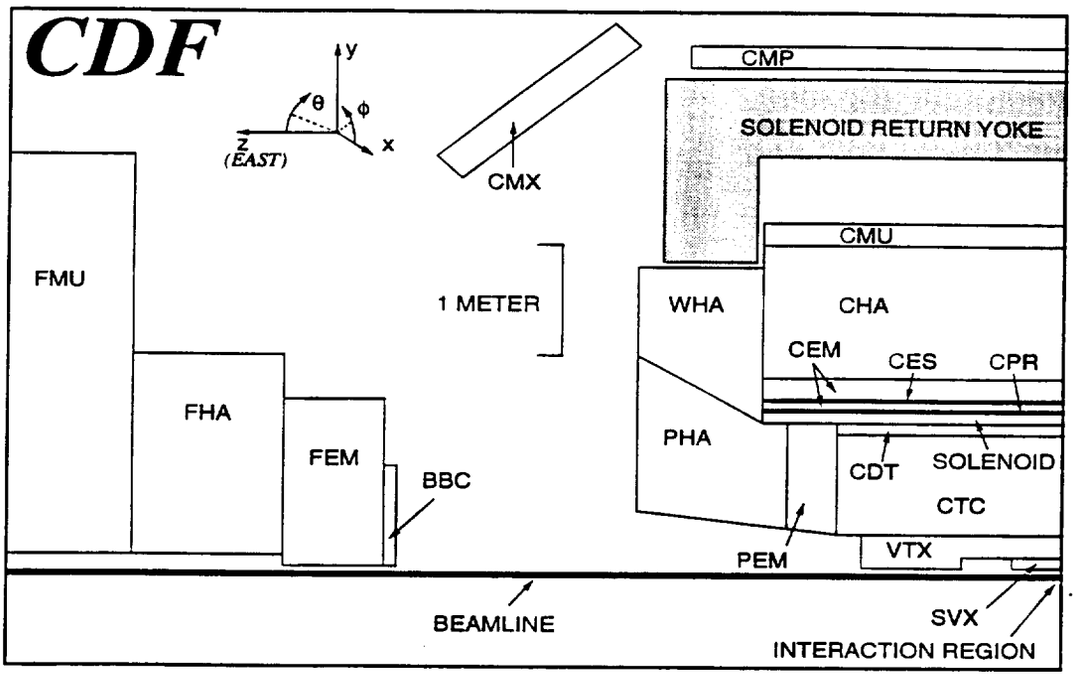

Wimpenny & Winer Fig. 7

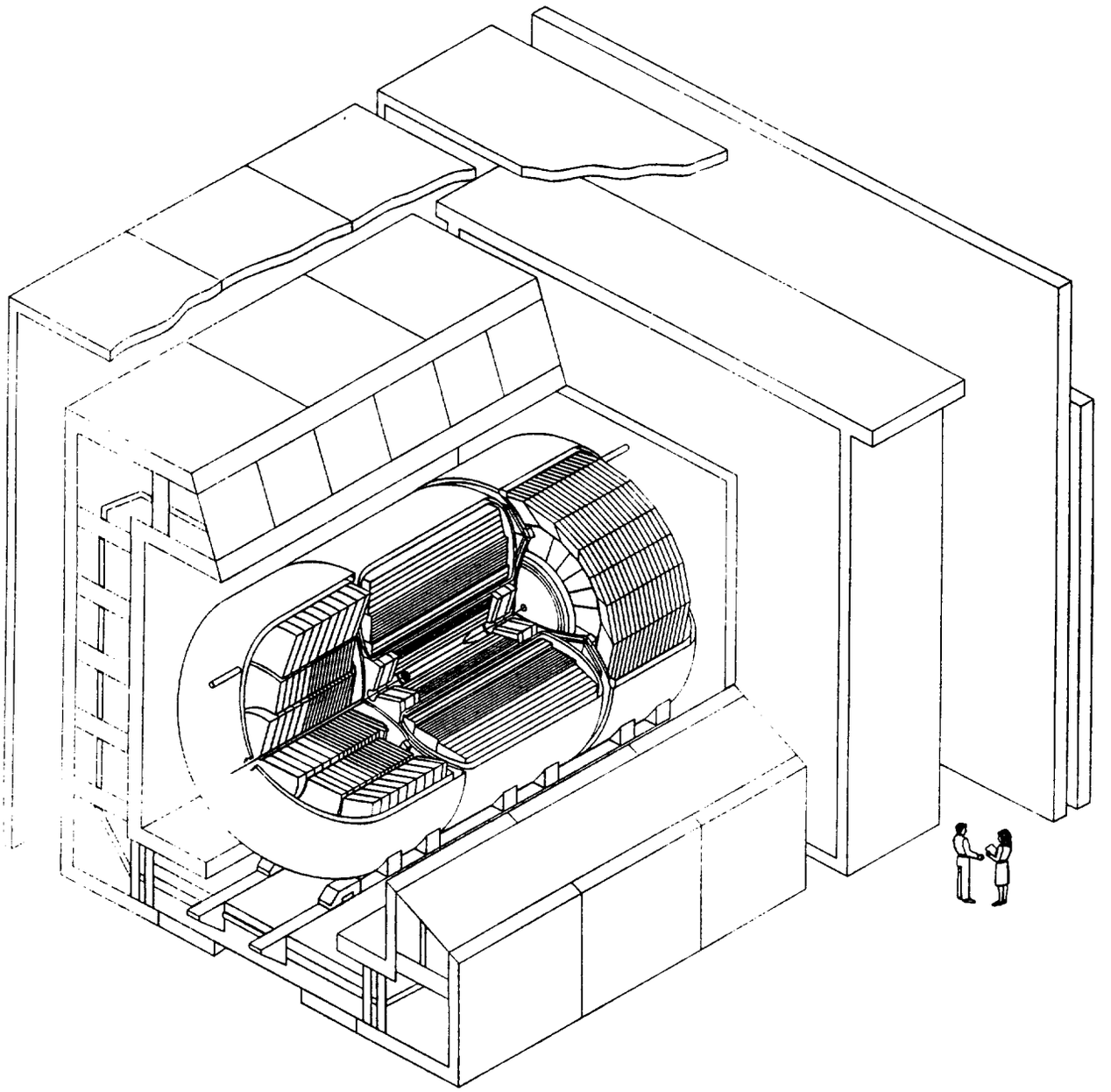

Wimpenny & Winer Fig. 8

Muon

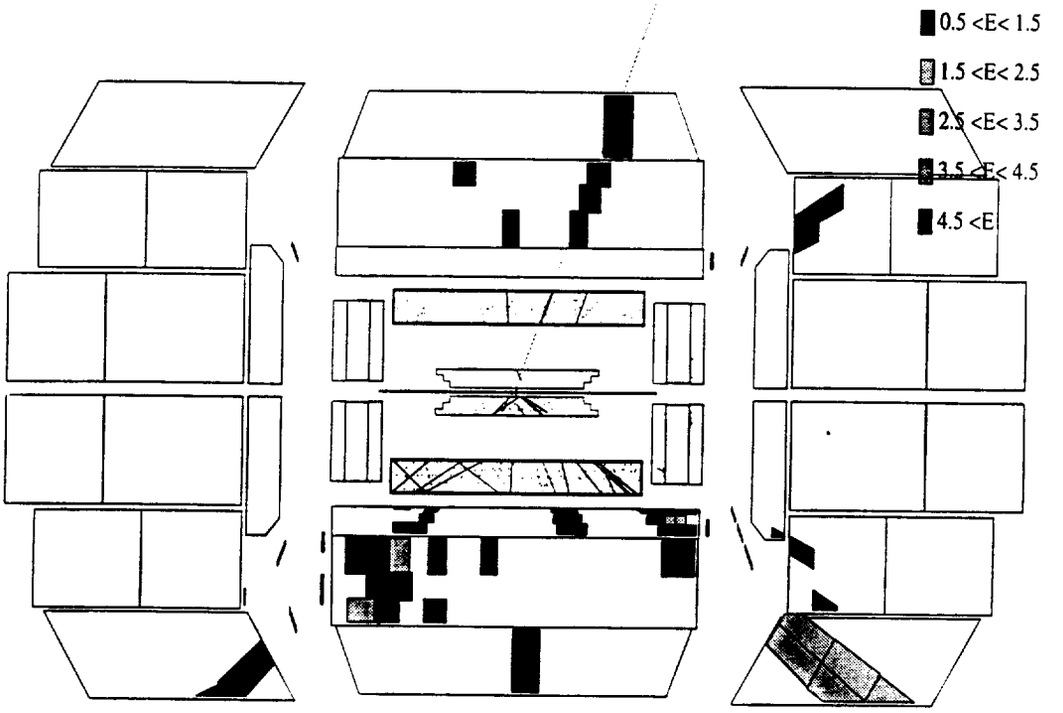

Jet 1

Jet 2

Electron

Wimpenny & Winer Fig. 9

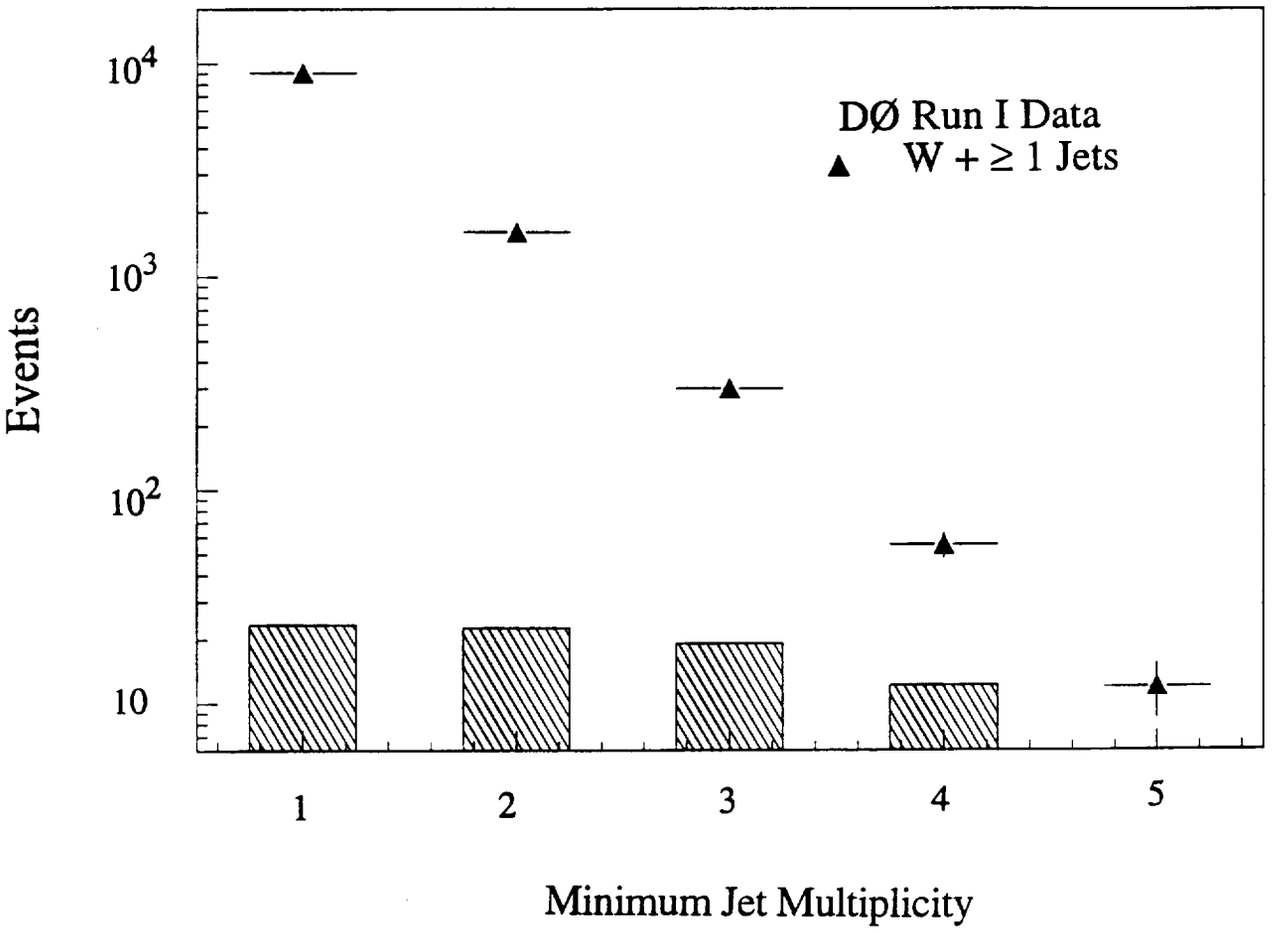

Wimpenny & Winer Fig. 10

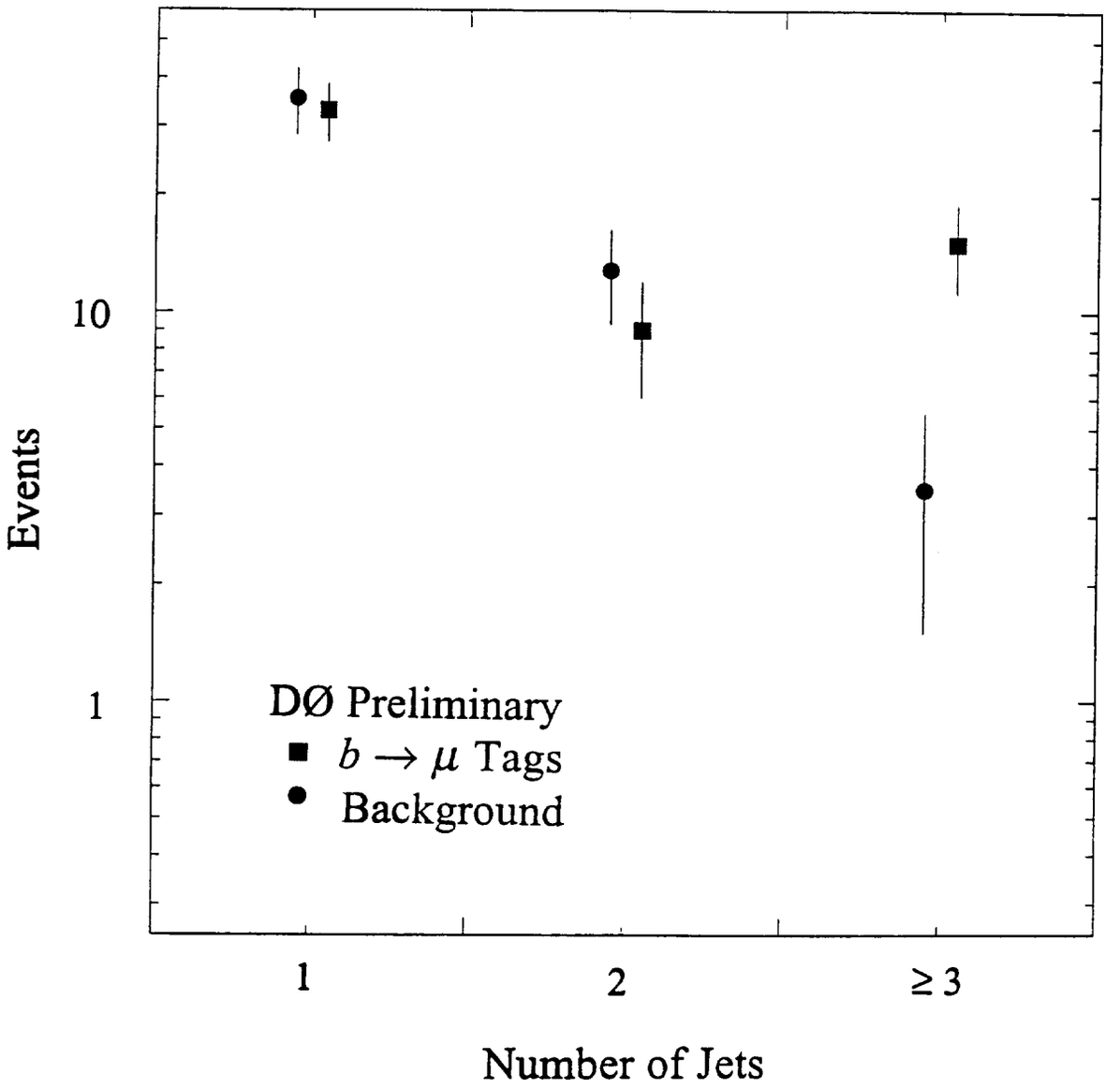

Wimpenny & Winer Fig. 11

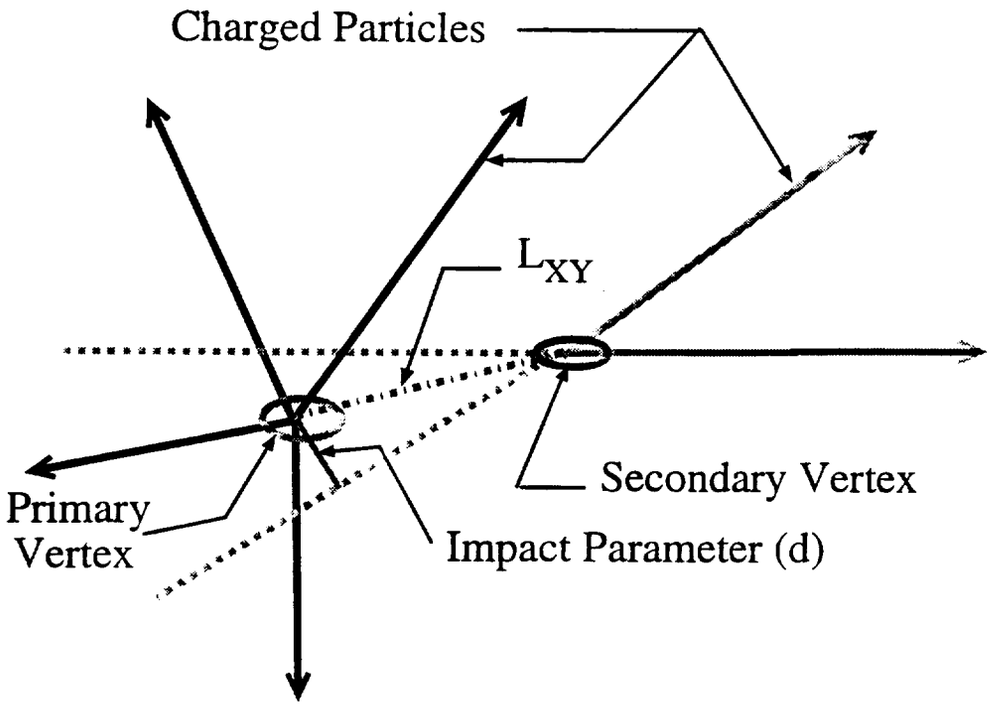

Wimpenny & Winer Fig. 12

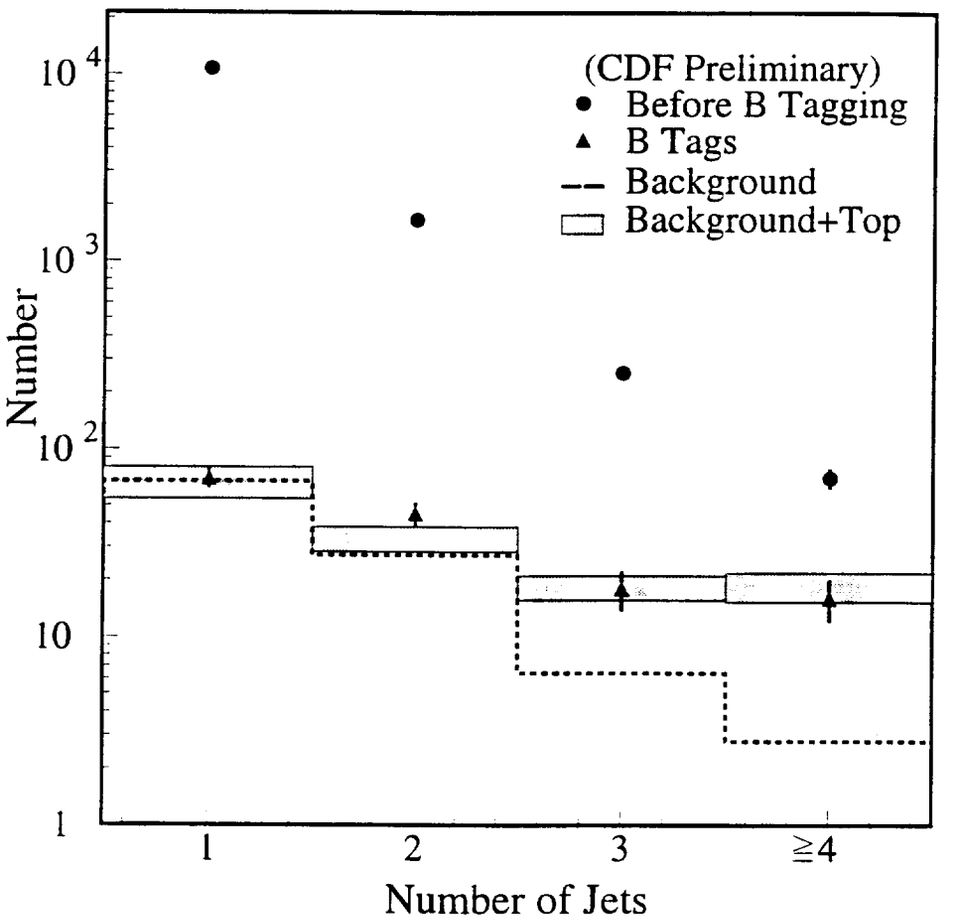

Wimpenny & Winer Fig. 13

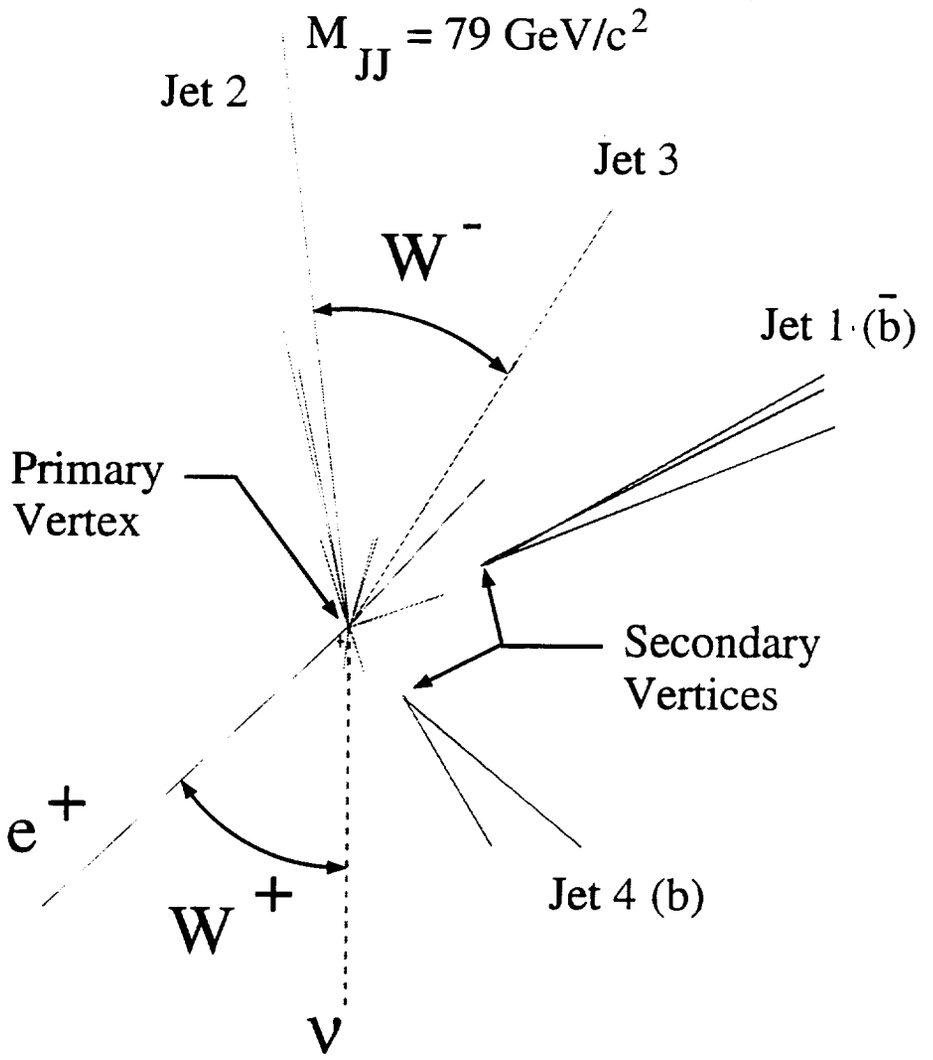

Wimpenny & Winer Fig. 14

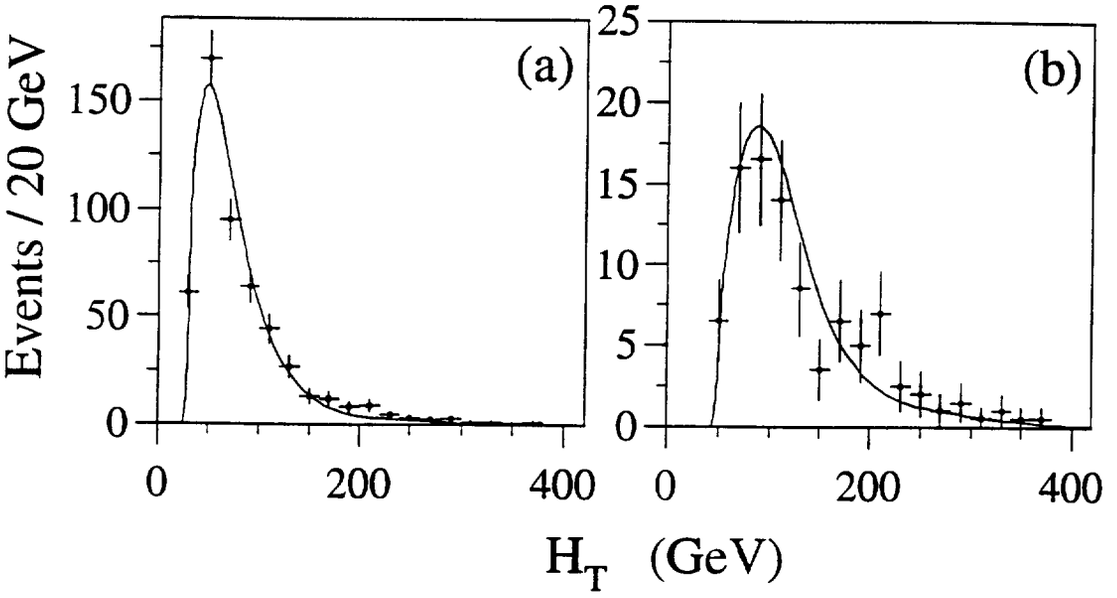

Wimpenny & Winer Fig. 15

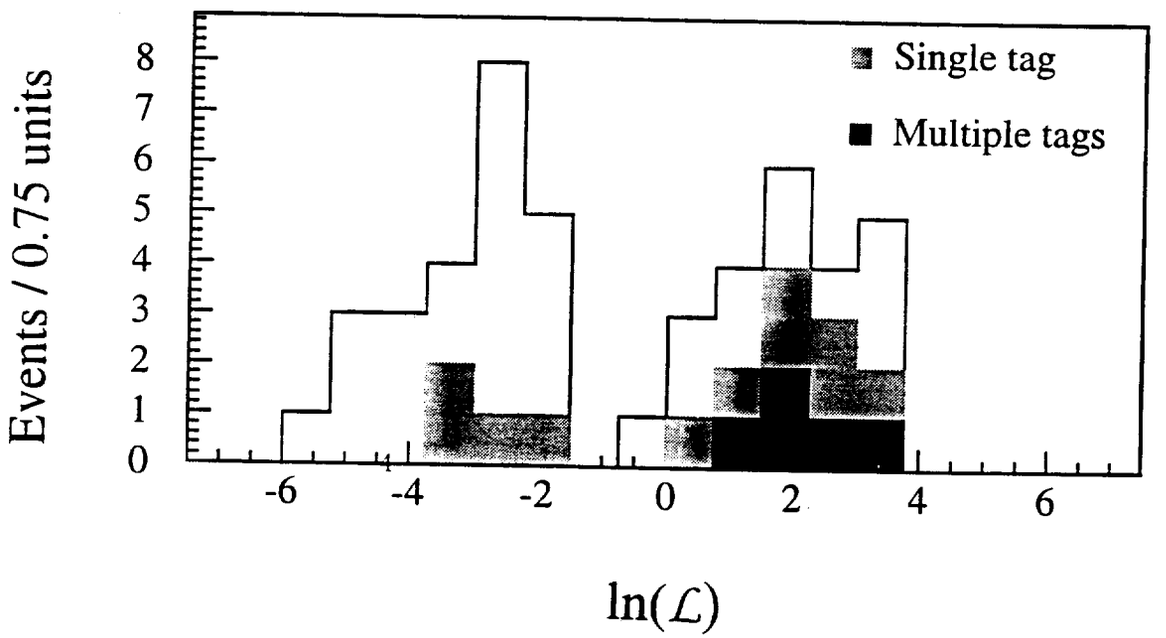

Wimpenny & Winer Fig. 16

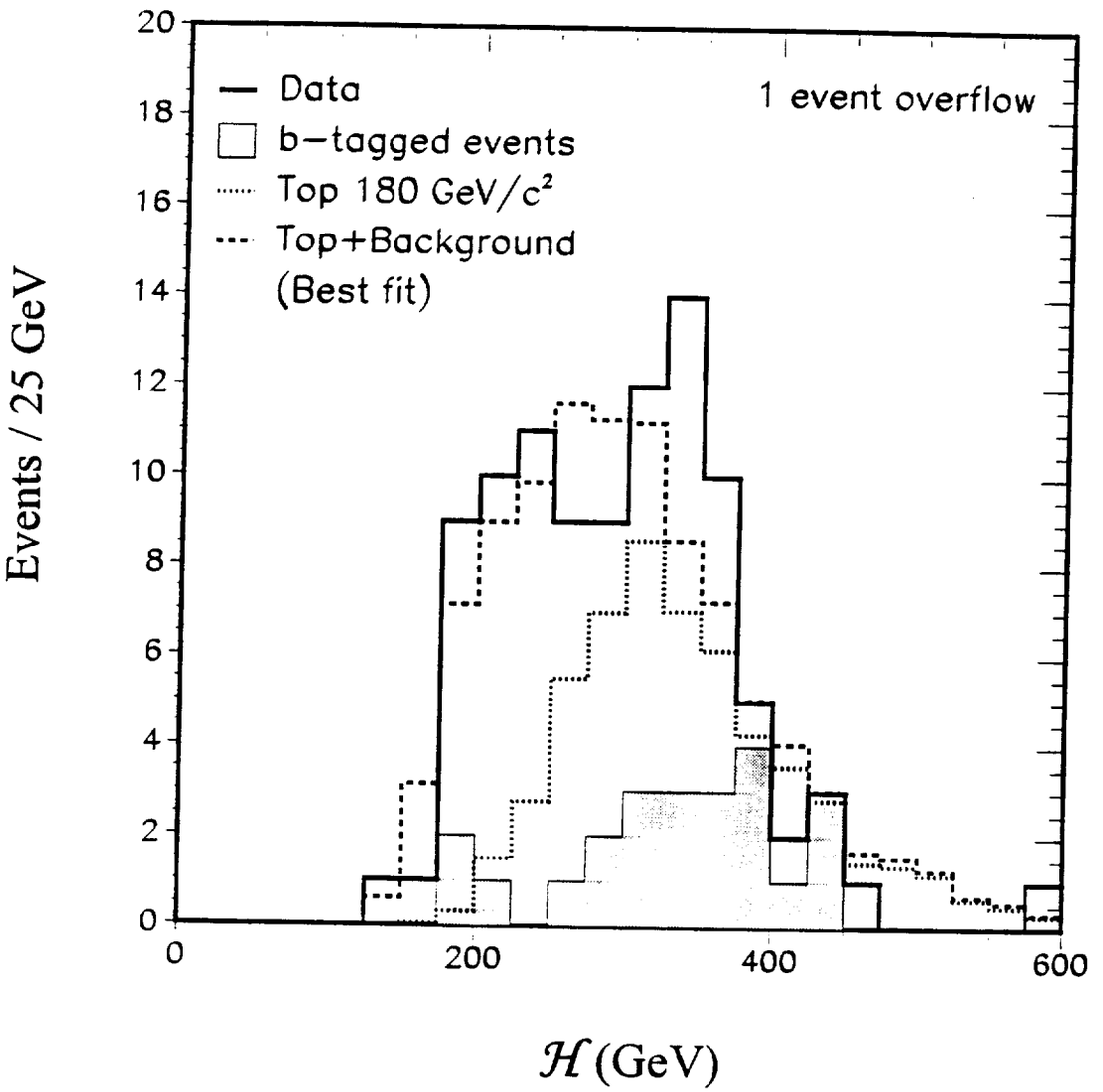

Wimpenny & Winer Fig. 17

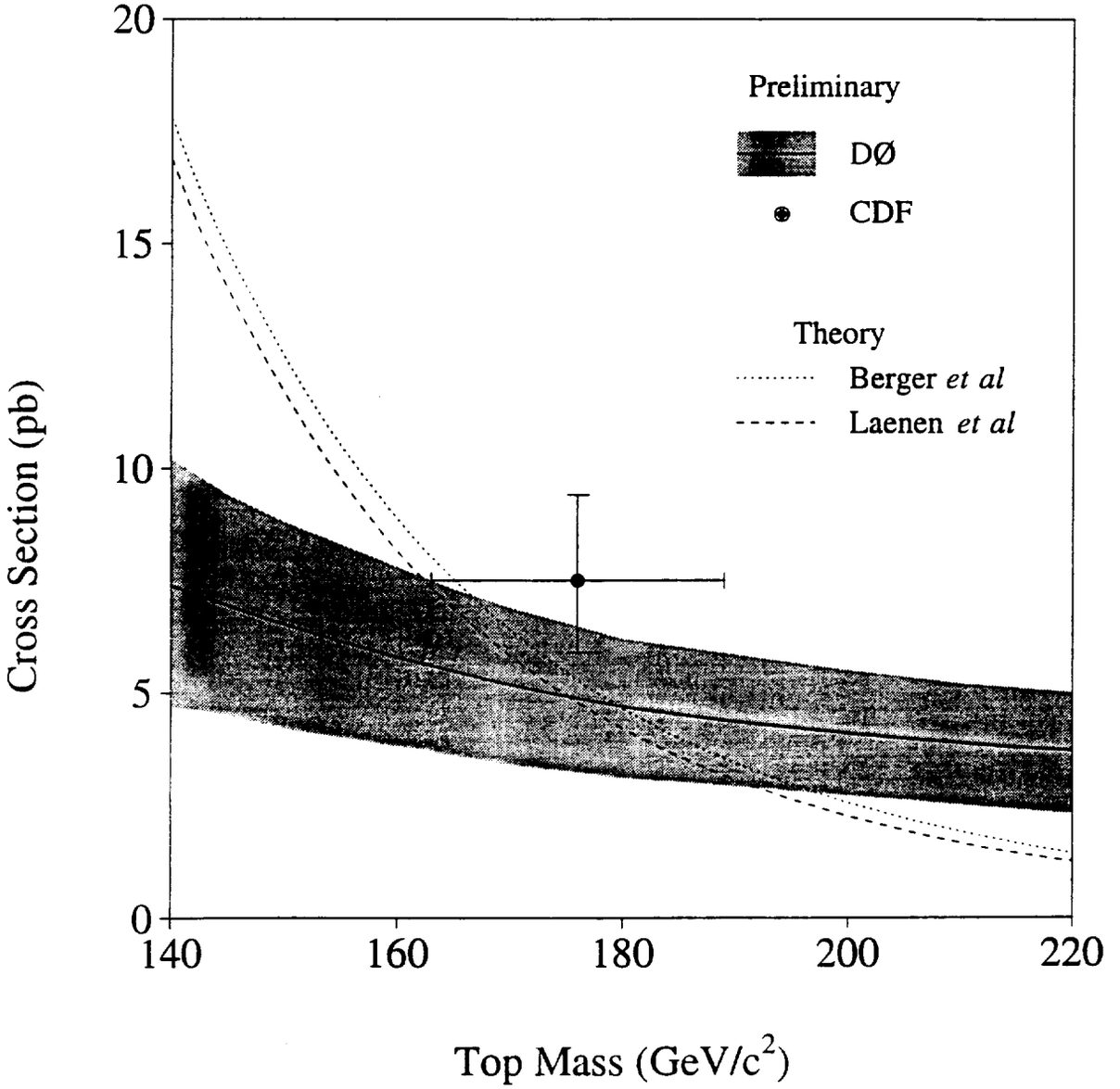

Wimpenny & Winer Fig. 18

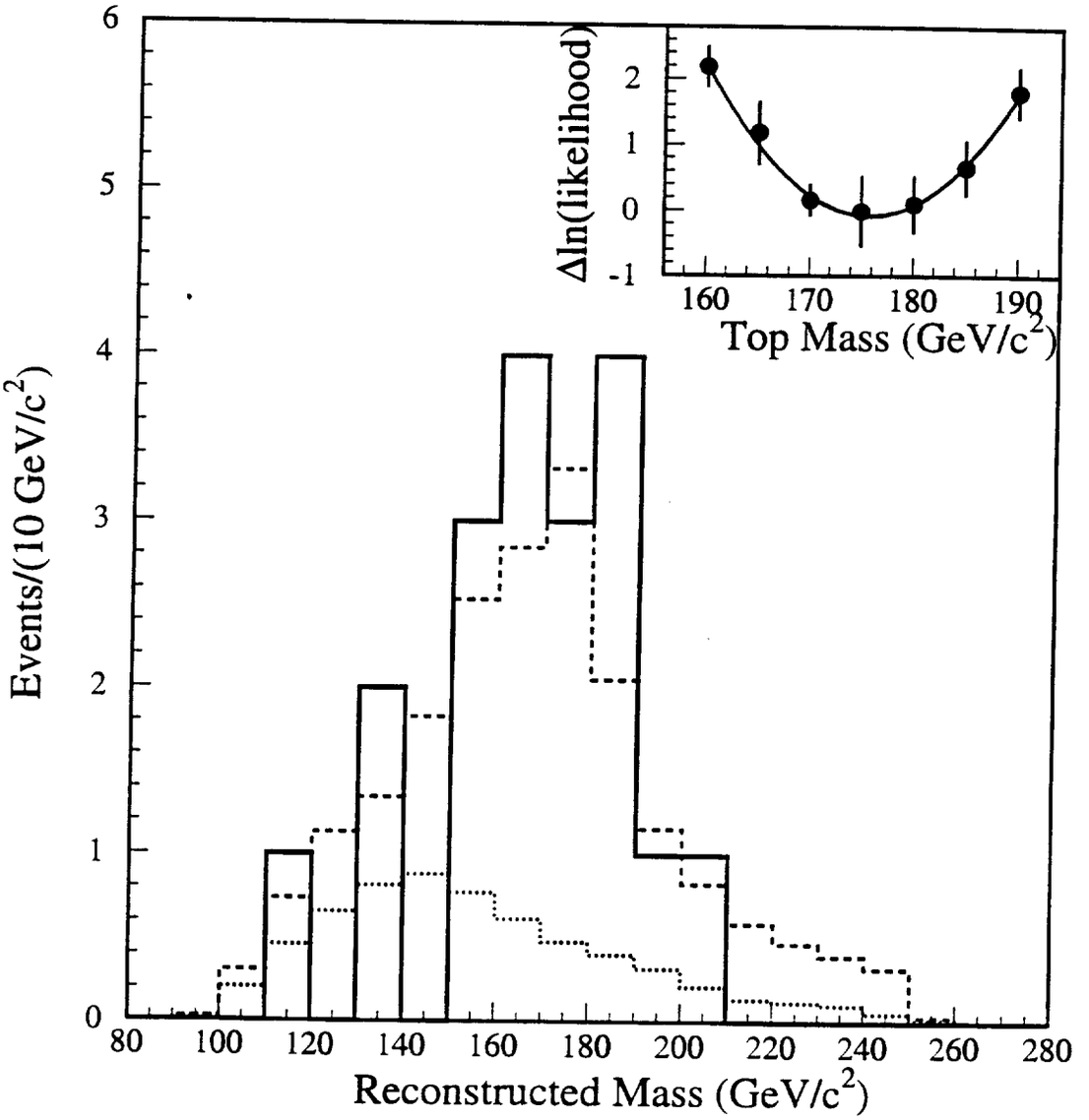

Wimpenny & Winer Fig. 19

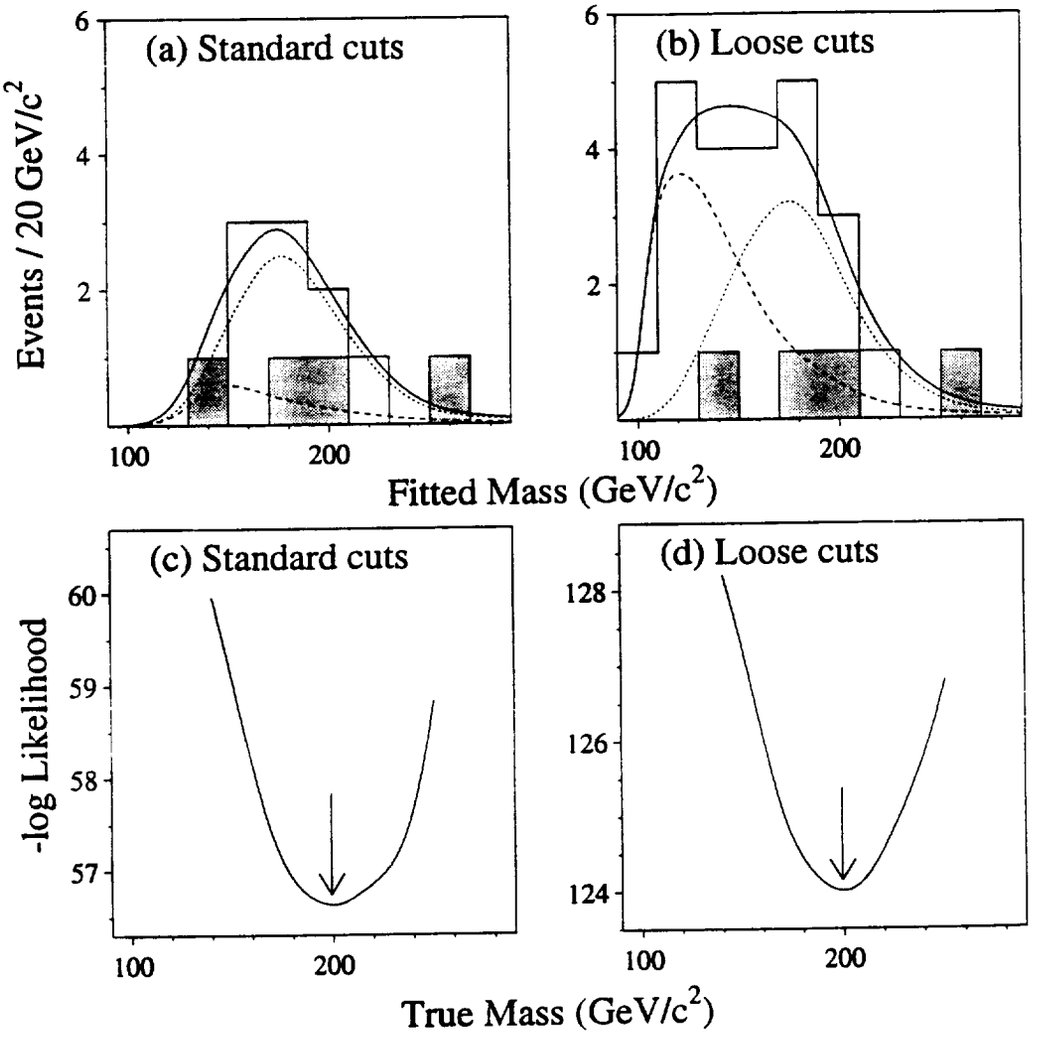

Wimpenny & Winer Fig. 20

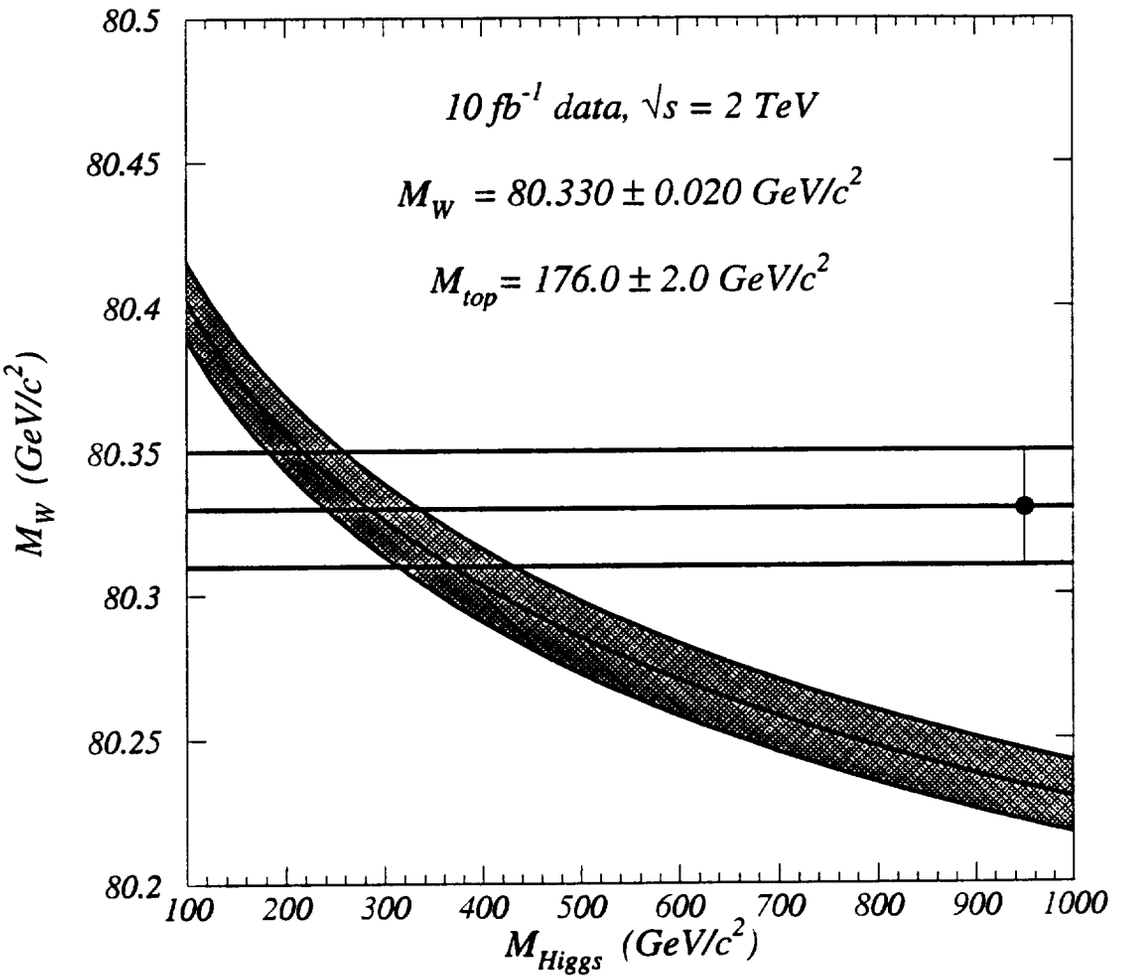

Wimpenny & Winer Fig. 21